

NPS ARCHIVE
1966
MURPHY, J.

THE EFFECTS OF NONSTEADY FLOW
ON THE PRESSURE DISTRIBUTION ABOUT
A CIRCULAR CYLINDER

JOHN COWDEN MURPHY

LIBRARY
NAVAL POSTGRADUATE SCHOOL
MONTEREY, CALIF. 93940

DUDLEY KNOX LIBRARY
NAVAL POSTGRADUATE SCHOOL
MONTEREY CA 93943-5101

This document has been approved for public
release and sale; its distribution is unlimited.

DUDLEY KNOX LIBRARY
NAVAL POSTGRADUATE SCHOOL
MONTEREY CA 93943-5101

THE EFFECTS OF NONSTEADY FLOW ON THE PRESSURE
DISTRIBUTION ABOUT A CIRCULAR CYLINDER

by

John Cowden Murphy
Lieutenant, United States Navy
B.S., Texas A. & M. University, 1958

Submitted in partial fulfillment
for the degree of

AERONAUTICAL ENGINEER

from the

UNITED STATES NAVAL POSTGRADUATE SCHOOL
May 1966

PS Archive
966
Murphy, J.

~~Th...~~
~~M...~~
~~...~~

UNIVERSITY OF TORONTO
LIBRARY

ABSTRACT

Nonsteady flow is an inherent problem in all fields of aerodynamics. The present work is an experimental investigation of the effects of large scale flow disturbances on the pressure distribution about a transverse circular cylinder. The nonsteady flow in this study was obtained by use of a rotating shutter valve to superimpose a sinusoidally varying velocity component on a mean stream. The frequency of the velocity oscillation covers the range of from 2.0 to 90.0 cycles per second, with amplitudes ranging from 10 to 40 percent of the mean freestream velocity.

Both the mean pressure distributions and the instantaneous surface pressure variations were studied for flows in the subcritical and transcritical Reynolds number ranges. Results show that the mean surface pressure is affected most in the high transcritical Reynolds number range at low oscillation frequencies. Here the effect is a reduction of the critical Reynolds number. An effect of low oscillation frequencies on the instantaneous pressure variations consists of a phase shift between the freestream velocity and the velocity near the wall. At high oscillation frequencies this phase shift does not occur, however random fluctuations in the surface pressure are introduced at all angular positions on the cylinder surface.

TABLE OF CONTENTS

Section	Page
1. Introduction	13
2. Experimental Equipment and Procedures	15
Wind Tunnel	15
Rotating Shutter Valve	17
Test Section	19
Cylinder Model	24
Instrumentation	26
3. Experimental Results and Discussion	36
4. Conclusions	54
5. Acknowledgement	56
6. Bibliography	57
Appendix I	59

LIST OF ILLUSTRATIONS

Figure		Page
1.	Schematic Drawing of Wind Tunnel	16
2.	Photograph of Rotating Shutter Valve	18
3.	Photograph of Wind Tunnel Test Section	20
4.	Photograph of Wind Tunnel Test Section	22
5.	Typical Wind Tunnel Test Section Velocity Profile	23
6.	Photograph of Hot Wire Anemometer	25
7.	Photograph of Cylinder Model Mounted in the Test Section	27
8.	Schematic Drawing of Pressure Transducer Installation	28
9.	Pressure Transducer Calibration Curve	29
10.	Pressure Transducer Gravity Effect Calibration Curve	30
11.	Photograph of Instrumentation and Readout Equipment	32
12.	Schematic Diagram of the Instrumentation Circuitry	33
13.	Hot Wire Anemometer Calibration Curve	34
14.	Steady Flow Surface Pressure Distributions	38
15.	Mean Surface Pressure Distributions	39
	$N_{Re} = 1.95 \times 10^5$	
	$f = 2.0$ and 29.0 cps	
16.	Mean Surface Pressure Distributions	41
	$N_{Re} = 2.45 \times 10^5$	
	$f = 2.0, 12.4,$ and 15.0 cps	

Figure		Page
17.	Mean Surface Pressure Distributions $N_{Re} = 2.45 \times 10^5$ $f = 18.0$ and 37.0 cps	42
18.	Mean Surface Pressure Distributions $N_{Re} = 2.45 \times 10^5$ $f = 53.0$ and 90.0 cps	43
19.	Mean Surface Pressure Distributions $N_{Re} = 3.23 \times 10^5$ $f = 2.0$ and 3.4 cps	44
20.	Mean Surface Pressure Distributions $N_{Re} = 3.23 \times 10^5$ $f = 12.2$ and 29.0 cps	45
21.	Mean Surface Pressure Distributions $N_{Re} = 3.43 \times 10^5$ $f = 2.0, 7.3,$ and 12.5 cps	47
22.	Mean Surface Pressure Distributions $N_{Re} = 3.52 \times 10^5$ $f = 2.0$ and 12.4 cps	48
23.	Oscilloscope Traces of the Freestream Velocity and Cylinder Surface Pressure $N_{Re} = 1.95 \times 10^5$ $f = 2.0$ cps	50

Figure

Page

24. Oscilloscope Traces of the Freestream Velocity and
Cylinder Surface Pressure

53

$$N_{Re} = 3.52 \times 10^5$$

$$f = 12.4 \text{ cps}$$

LIST OF TABLES

Table		Page
1.	Hot Wire Anemometer Calibration and Freestream Turbulence Intensity	35
2.	Experimental Operating Conditions	37
3.	Mean Pressure Coefficients	60

LIST OF SYMBOLS

Symbol	Definition	Units
C_p	Pressure Coefficient $= \frac{P - P_s}{\frac{\rho \cdot U_\infty^2}{2}}$	---
D	Cylinder Diameter	in.
e_p	Electrical signal corresponding to p	volts
e_u	Electrical signal corresponding to u	volts
E_p	Electrical signal corresponding to P	volts
E_u	Electrical signal corresponding to U	volts
$E_{\bar{u}}$	Electrical signal corresponding to \bar{U}	volts
E_{u_∞}	Electrical signal corresponding to U_∞	volts
f	Frequency of freestream velocity fluctuations	cycles/sec.
N_{Re}	Reynolds number $= \frac{U_\infty D}{\nu}$	---
N_{ua}	Dimensionless velocity amplitude $= \frac{\Delta U}{U_\infty}$	---
p	Instantaneous cylinder surface pressure	lb./in. ²
P	Mean cylinder surface pressure	lb./in. ²
P_s	Test section static pressure	lb./in. ²
U	Instantaneous freestream velocity	ft./sec.

Symbol	Definition	Units
\bar{U}	Amplitude of freestream turbulence fluctuations (root mean square value)	ft./sec.
U_{∞}	Freestream mean velocity	ft./sec.
\bar{U}/U_{∞}	Freestream turbulence intensity (root mean square value)	---
ΔU	Amplitude of freestream velocity fluctuations	ft./sec.
ν	Kinematic viscosity	ft. ² /hr.

1. Introduction.

Flow about a circular cylinder has been the subject of many investigations both analytical and experimental, nevertheless these studies have been mostly confined to the problems dealing with steady, low turbulence level streams. Areas of interest still remain to be investigated in the field of nonsteady flows. To some degree all aerodynamic flows are influenced by nonsteadiness. In the investigation of rotating stall in compressors, aerodynamic flutter and the study of accelerating bodies, large amplitude disturbances are an integral part of the problem. The present study was undertaken to investigate the effects of an oscillating freestream on the pressure distribution about a circular cylinder, transverse to the flow.

The potential flow theory solution for the distribution of pressure about a cylinder is well known and the results of experiments to determine the pressure distribution in steady, incompressible, viscous flows have been published many times. [1, 2, 3, 4] * The pressure distribution and therefore the drag coefficient on circular cylinders has been shown to be a function of the Reynolds number, which is a dimensionless number expressing the ratio of inertial to viscous forces in flows over geometrically similar bodies. In the subcritical Reynolds number range the boundary layer is laminar up to the separation point, which is located on the forward portion of the cylinder. Schlichting shows that as the Reynolds number is increased above 2.0×10^5 , a sharp decrease in the drag coefficient occurs until, at approximately $N_{Re} = 5.0 \times 10^5$, the drag coefficient again be-

* Numbers in brackets refer to the references listed in the Bibliography

comes essentially constant. [1] It is in this transition region that the pressure distribution is significantly changed. Above a critical Reynolds number of about 5.0×10^5 , a turbulent boundary layer is established and the separation point becomes located on the downstream side of the cylinder. It is known however that, in addition to the Reynolds number effect discussed above, the freestream turbulence intensity also affects the flow pattern.

Fage and Falkner have done extensive work on the determination of the characteristics of the flow about a circular cylinder in a steady stream. [2, 3, 4] Included in their investigations was a determination of the pressure distribution around the cylinder at very low wind tunnel turbulence levels over a Reynolds Number range of from 0.6×10^5 to 4.0×10^5 . In their later work Fage and Falkner investigated the effects of small freestream disturbances on the pressure distribution, boundary layer and drag coefficient. Their method for introducing disturbances on the wind tunnel stream consisted of placing a square meshed rope netting across the wind tunnel 3 feet ahead of the model. Although the intensity of the induced turbulence was not measured, this experiment demonstrated that the critical Reynolds Number was significantly decreased in the disturbed flow. Gerrard has further discussed this effect in connection with the reported experimental data on drag coefficient in low turbulence level wind tunnels. [5]

The investigation of the flow about circular cylinders in a nonsteady stream has been limited. Schmidt and Spitzer have studied the problem of nonsteady aerodynamic loads on a cantilevered circular cylinder in a steady flow. [6, 7] Glauert has investigated the flow over cylinders which oscillate

in a direction transverse to the freestream flow. [8] Hori has measured the mean and fluctuating velocities in the boundary layer of a circular cylinder oscillating in the direction of the wind tunnel stream. [9] Due to the mechanical method of oscillating the cylinder adopted by Hori, his study is limited to a maximum frequency of 3.5 cycles per second. Vidal, while investigating laminar separation from a moving wall, has obtained pressure plots around a rotating cylinder. [10]

The objective of the present work is to investigate the effects of large amplitude oscillating flows on the pressure distribution about a transverse circular cylinder in the subcritical and lower transcritical Reynolds Number range (1.9×10^5 to 3.53×10^5). An oscillating flow is defined as a flow in which a sinusoidally varying velocity is superimposed on a constant freestream. The freestream oscillation frequency range investigated covered from 2 to 90 cycles per second. The amplitude of the velocity disturbances covered the range of 10.5 to 40.6 percent of the mean freestream velocity.

2. Experimental Equipment and Procedures.

Wind Tunnel

The study was conducted in the low-speed, oscillating flow wind tunnel located in the Aeronautics Laboratories of the United States Naval Postgraduate School. This wind tunnel is of open circuit design. The test section is 24 inches square and $223\frac{1}{2}$ inches long. Figure 1 is a plan view of the wind tunnel. The entire tunnel with the exception of the test section is constructed of one quarter inch steel plate. The inlet section is eight feet square. Three high solidity screens are located in the inlet section for re-

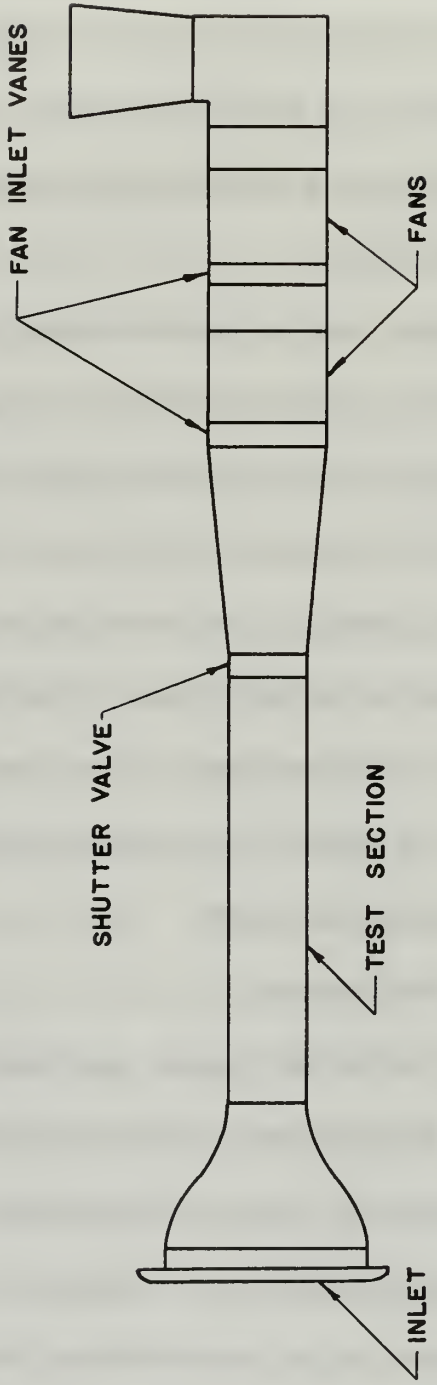


FIGURE 1

PLAN VIEW OF WIND TUNNEL

duction of test section turbulence. These screens are pretensioned by spring loaded frames which are recessed in the walls of the inlet. The nozzle section of the tunnel has a contraction ratio of 16:1. The screens and contraction ratio produce test section freestream turbulence levels of 0.343 to 0.478 percent.

The wind tunnel is driven by two Joy Axivane Fans in series, each of which has an internal 100 horsepower, direct connected, 1750 rpm motor. The fan blades are adjustable through a pitch range of 25 to 55 degrees to provide a wide operating range. Two sets of variable inlet vanes, one located directly in front of each fan, give external control of the test section velocity. These vanes are of multileaf design and preswirl the air in the direction of fan rotation to reduce the fan capacity. For the present work the fan blades were set so that control by the inlet vanes and the running of either one or both fans provided a test section steady flow velocity range of 88-250 feet per second. The outer case of the fans is also one quarter inch thick steel sheet. The heavy construction of the wind tunnel is necessary to withstand the induced vibration from the oscillating flow.

Rotating Shutter Valve

Several methods of obtaining an oscillating flow have been employed. In his investigation of the laminar boundary layer of a flat plate Nickerson approached the problem in much the same manner as Hori. [11] Nickerson also encountered mechanical difficulties when he tried to extend his investigation to high oscillation frequencies. Feiler and Yeager have employed a siren assembly to produce an oscillating flow in their investigations into



FIGURE 2
PHOTOGRAPH OF
ROTATING SHUTTER VALVE

the effects of large amplitude oscillations on heat transfer rates. [12, 13] They have achieved oscillation frequencies as high as 100 cycles per second.

The most successful method of obtaining an oscillating flow with large amplitude and frequency ranges was employed by Miller in his investigation of flat plate boundary layer transition. [14] By employing a rotating shutter valve downstream of the wind tunnel test section, a sinusoidal variation of velocity is superimposed on the mean flow. This approach has been employed in the present investigation. The shutter valve in this wind tunnel is basically the same as that described in Ref. 14. Figure 2 is a photograph of the rotating shutter valve. However, in the present installation the shutter is driven by a five horsepower variable speed electric motor. An intermediate shaft between the variable speed motor and the shutter valve allows a wide variety of pulley ratios. This drive arrangement gives an oscillation frequency range of from two cycles per second up to the first critical frequency of 933 cycles per second. The frequency of oscillation is obtained from a magnetic pickup whose output is read from a Berkeley decade counter. The magnetic pickup, seen in Figure 2, is mounted outboard of one of the shutter valve shafts.

Various widths of shutter valve blades may be employed to obtain oscillation amplitudes from 8 to 92 percent of freestream velocity.

Test Section

The test section is shown in Figure 3. The top and bottom of the test section are single piece two inch thick aluminum plates. Each side of the section is fabricated of three sheets of two inch thick stress relieved lucite

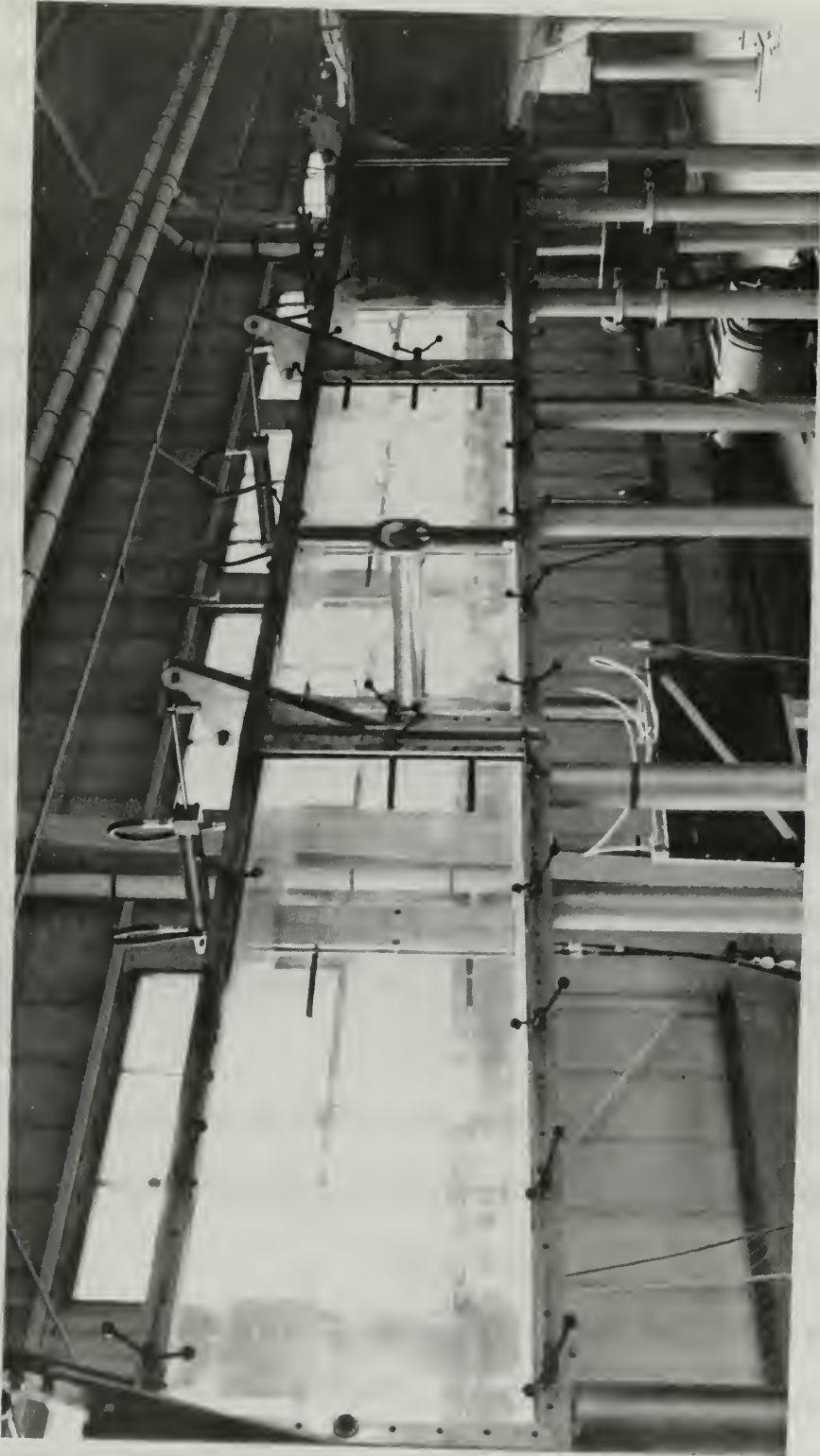


FIGURE 3
PHOTOGRAPH OF WIND TUNNEL
TEST SECTION

plate. The three windows on the console side of the test section are hinged and may be hydraulically opened. Figure 4 shows the test section with these windows open. The heavy construction of the test section is intended to minimize deflection due to the variation of static pressure.

Prior to the installation of the circular cylinder model, surveys were conducted to determine the velocity profiles of the wind tunnel test section. Velocity surveys were conducted at two stations, the first at 74 inches from the upstream end of the test section, the second at 148 inches. A standard pitot-static tube and an upright manometer were used for these surveys. Surveys were made at several test section velocities covering the entire velocity range of the wind tunnel (88-250 fps). Figure 5 shows the vertical center line velocity profile of the forward section for a freestream velocity of 120 fps. All of the velocity profiles indicated a velocity variation of less than $\pm 1\%$ across the test section to within approximately $2\frac{1}{2}$ inches from any wall at the forward station and $3\frac{1}{2}$ inches from the walls at the rear station.

A pitot-static tube and a 10 inch inclined draft gage having a slow response time were used as the primary measure of the mean test section velocity. For this study the pitot-static tube was located eight inches upstream of the model. A test section static pressure probe was flush mounted in the bottom of the tunnel ahead of the model.

A transistorized constant temperature hot wire anemometer, recently developed by Dr. J. A. Miller and Dr. G. D. Ewing of the U. S. Naval Post-graduate School, was employed in this investigation. The hot wire bridge circuit is coupled to an analogue computer circuit which inverts King's law

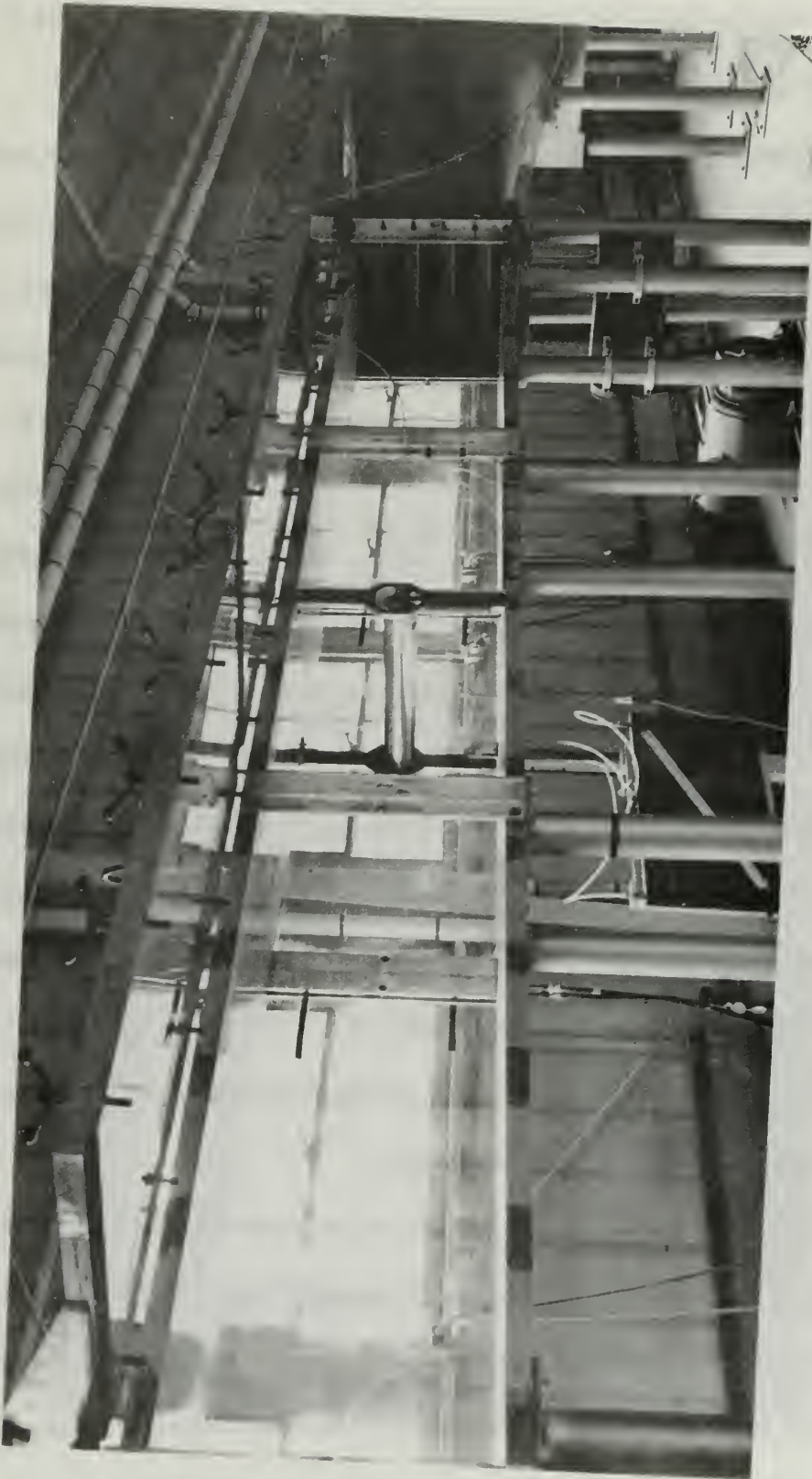


FIGURE 4

PHOTOGRAPH OF WIND TUNNEL
TEST SECTION

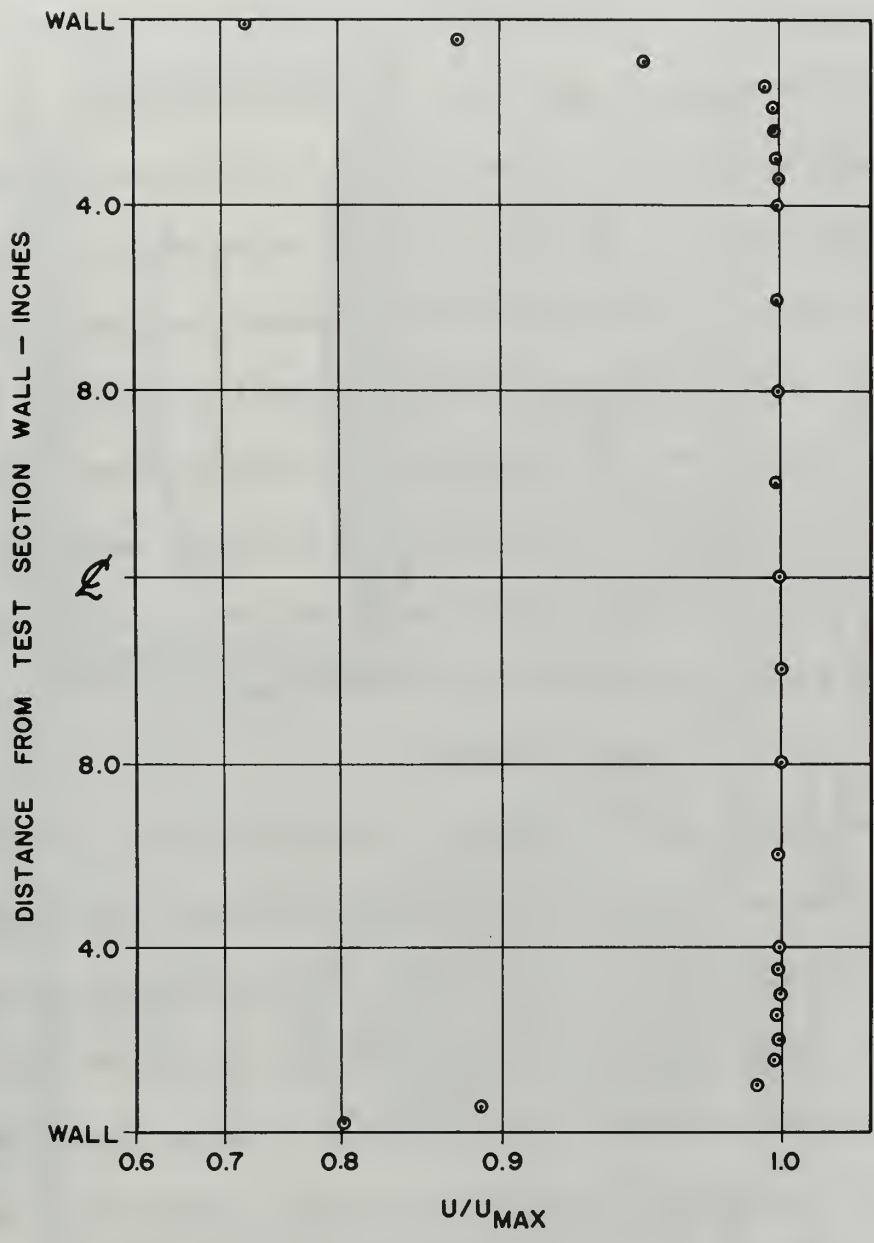


FIGURE 5

TYPICAL WIND TUNNEL TEST SECTION VELOCITY
 PROFILE 32 INCHES UPSTREAM OF
 CYLINDER MODEL $U_{MAX} = 120$ FT/SEC

and provides an output which is linear in velocity and zero for zero velocity. The inherent accuracy at the analogue transfer function is better than 0.5% over the operating range. Figure 6 shows the complete hot wire anemometer. The hot wire probe was made by embedding two jeweler's broaches in an epoxy plastic tip which in turn was mounted in a 1/4 inch stainless steel tube. The wires are copper plated to facilitate mounting on the probe and have effective filament lengths of from 0.080 to 0.090 inches. The direct current component of the hot wire anemometer, which is directly proportional to the mean velocity component, was measured with the meter contained in the instrument. The alternating current component of the output, which is directly proportional to the oscillating velocity component, was displayed on the upper beam of the Tektronix 555 Dual-Beam oscilloscope.

Cylinder Model

The circular cylinder model employed in this study is 3.91 inches in diameter. This diameter minimizes tunnel wall effects while maintaining the boundary layer thickness on the model adequate for future hot wire anemometer studies. Typical boundary layer thickness at the laminar separation point is of the order of 0.1 inches. The cylinder is of single piece aluminum construction and is supported on a 1/2 inch steel rod, which is coincident with the model centerline. The ends of the steel rod in turn rest in sealed ball bearings, which are pressed into 1/2 inch aluminum plates. Both the model and the supports are inside the test section. The ball bearing supports facilitate rotation of the cylinder from outside the test section. The entire length of the cylinder was finished by polishing with jeweler's rouge to min-

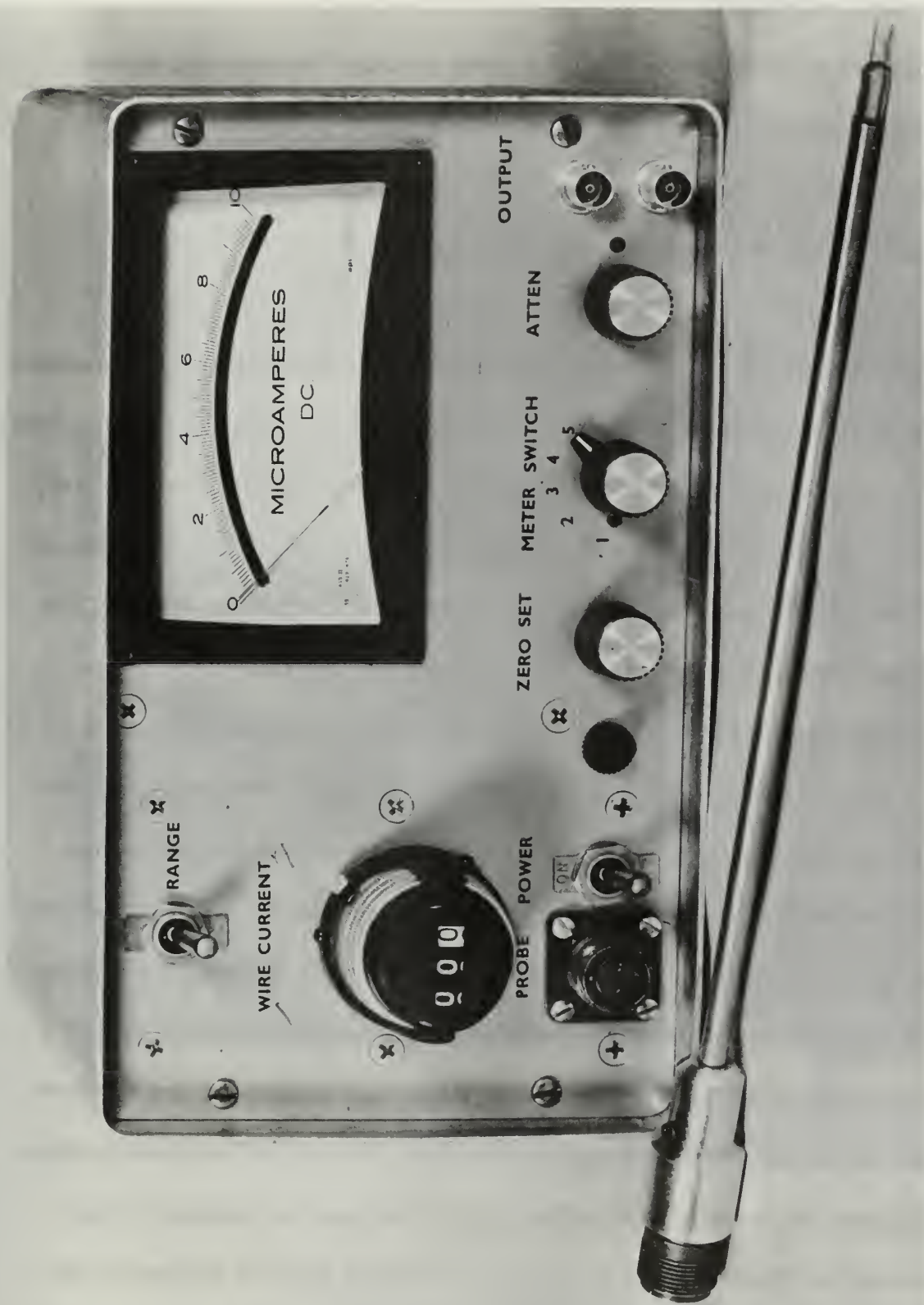


FIGURE 6
PHOTOGRAPH OF HOT WIRE ANEMOMETER

imize surface roughness.

The model, as shown in Figure 7, was mounted horizontally on the test section centerline at a point coincident with the longitudinal center of the test section. The ends of the model support plates were bolted to the top and bottom of the tunnel test section.

Instrumentation

A strain gage pressure transducer was used to measure surface pressure on the model. The operating range of the pressure transducer is ± 5.0 pounds per square inch gage pressure. The transducer was fixed to the inside well of the model as shown in Figure 8. A 1/16 inch diameter orifice was drilled through the cylinder wall to the pressure transducer diaphragm cavity. The total volume above the diaphragm was 0.0025 cubic inches.

The pressure transducer was calibrated, over the range of from -2.0 to +2.0 pounds per square inch gage pressure, after the model was mounted in the test section. Figure 9 shows the transducer calibration curve from which it is seen that the output is linear within 1.5 percent over the full calibration range and within 0.5 percent over the pressure range of the present investigation. It was found that the transducer sensitivity was such that the gravitational effect on the transducer diaphragm influenced the pressure output signal as the cylinder model was rotated. A calibration check of this effect yielded the curve shown in Figure 10. The angular position of the pressure orifice was measured by using an indexing mark on the end of the cylinder and a protractor mounted in the model support plate as is shown in Figure 7.



FIGURE 7

PHOTOGRAPH OF CYLINDER MODEL
MOUNTED IN TEST SECTION

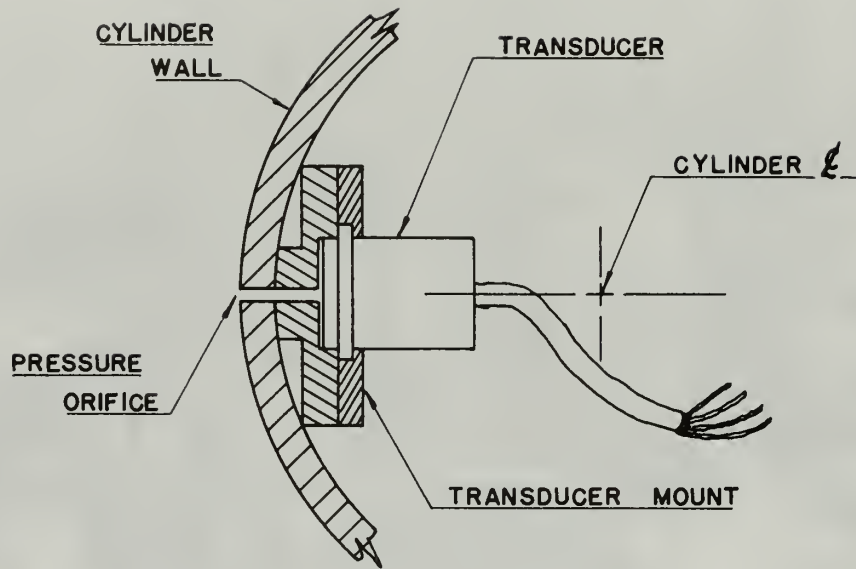
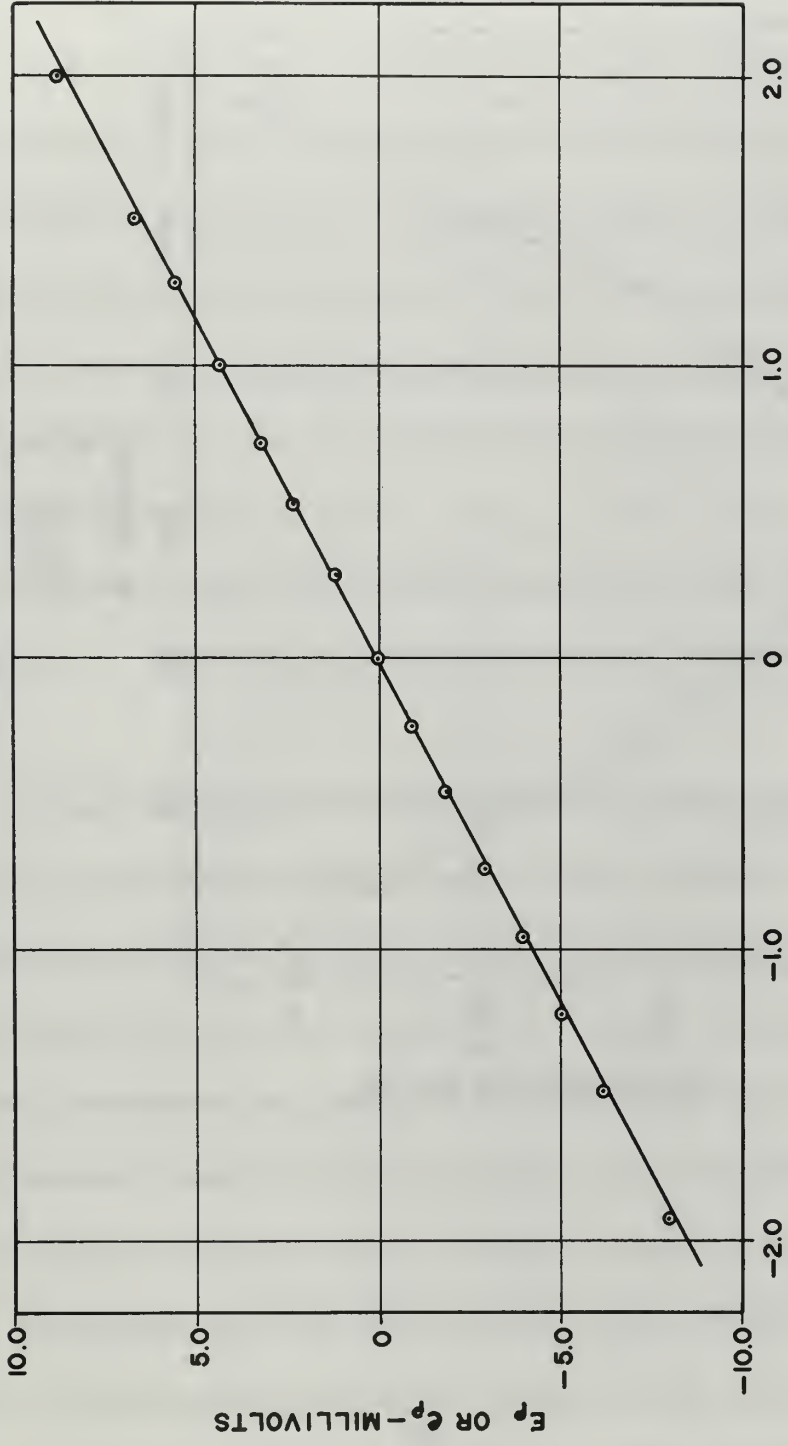


FIGURE 8

SCHEMATIC DRAWING OF PRESSURE
TRANSDUCER INSTALLATION



P - PSIG

FIGURE 9

PRESSURE TRANSDUCER CALIBRATION CURVE

EXCITATION VOLTAGE 8.25 VOLTS

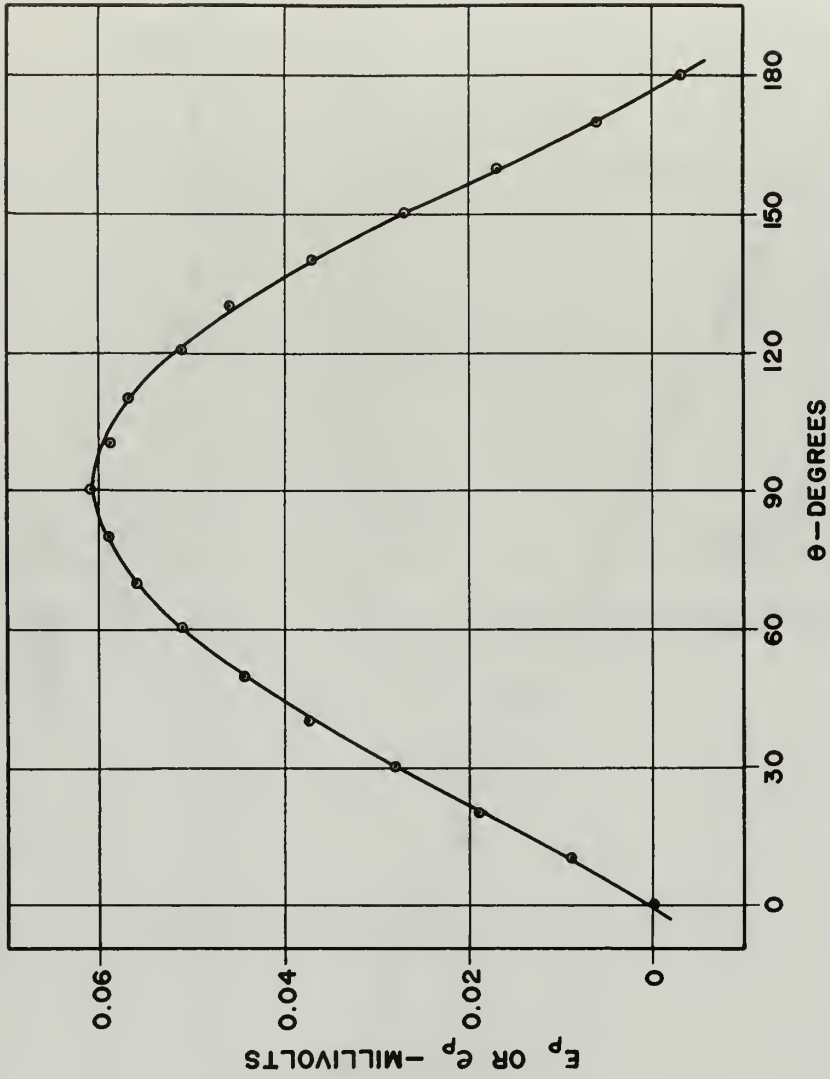


FIGURE 10

PRESSURE TRANSDUCER GRAVITY
EFFECT CALIBRATION CURVE

The direct current component of the transducer output was measured with an integrating digital voltmeter which is capable of resolving voltages as small as 0.1 microvolts. The alternating current component was amplified by a differential amplifier and displayed on the lower beam of the Tektronix oscilloscope. Incorporated in this oscilloscope is a sweep delay line between the upper and lower beams. With this feature, phase differences between the velocity and pressure traces may be accurately measured. The oscilloscope output was photographed with Tektronix C-12 camera and a Polaroid Land roll film back.

An overall view of the instrumentation and readout equipment is shown in Figure 11. Figure 12 is a schematic diagram of the instrumentation circuitry.

Several measurements were made in a steady stream to check the accuracy of the instrumentation. The hot wire anemometer was calibrated after installation in the test section. During this calibration run the freestream turbulence intensity was also measured. Figure 13 shows the results of the hot wire anemometer calibration. As reported above the turbulence intensity, in the velocity range of the present work, is from 0.343 to 0.484 percent. The freestream turbulence level at various velocities is listed in Table 1.

Measurements of the pressure distribution above the cylinder were made in a steady stream at various velocities over the Reynolds number range of from 1.95×10^5 to 3.52×10^5 . Prior to each pressure measurement run the pressure transducer was checked for zero output reading while positioned at the forward stagnation point. The cylinder surface was cleaned prior to

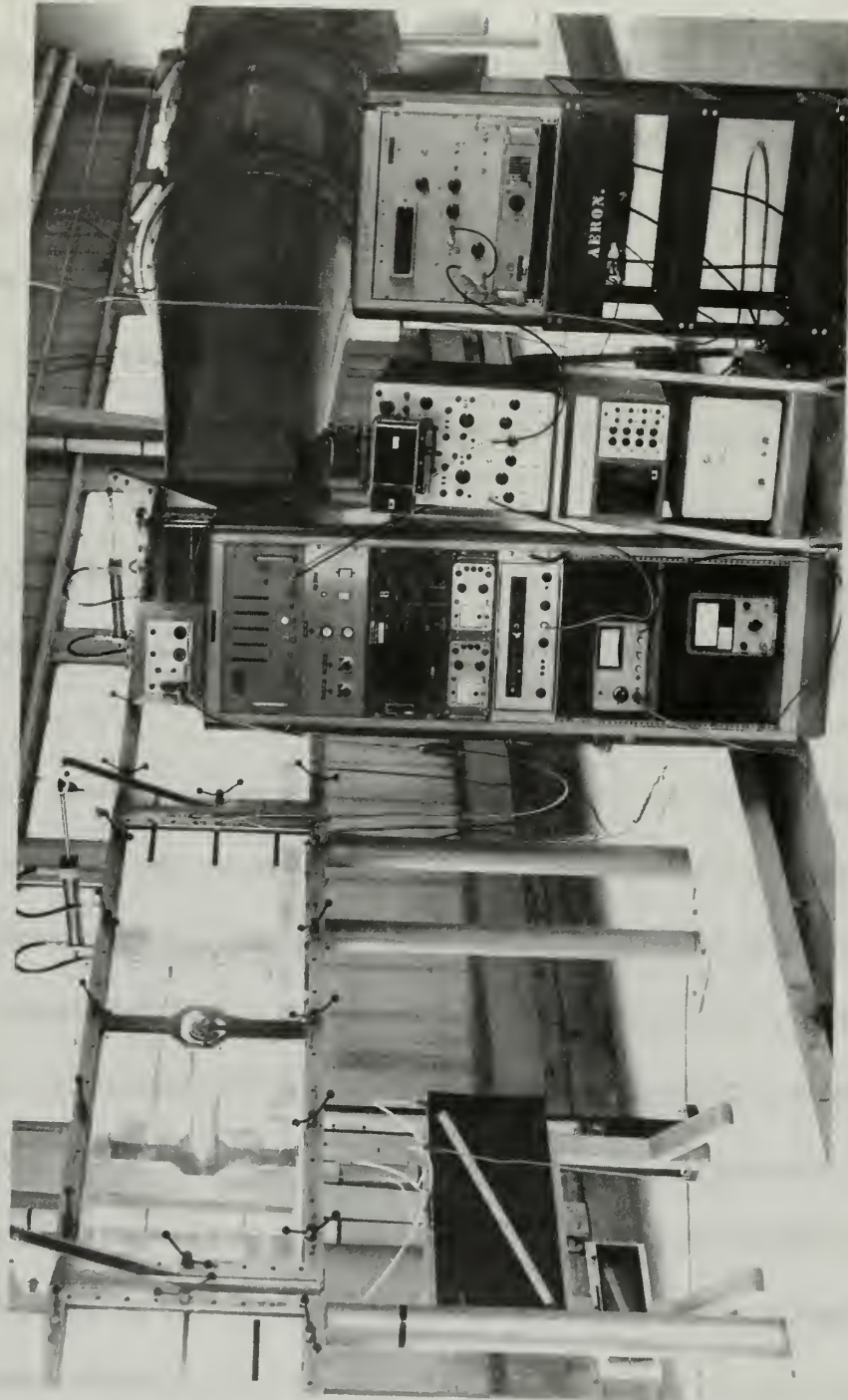


FIGURE 11
PHOTOGRAPH OF INSTRUMENTATION AND
READOUT EQUIPMENT

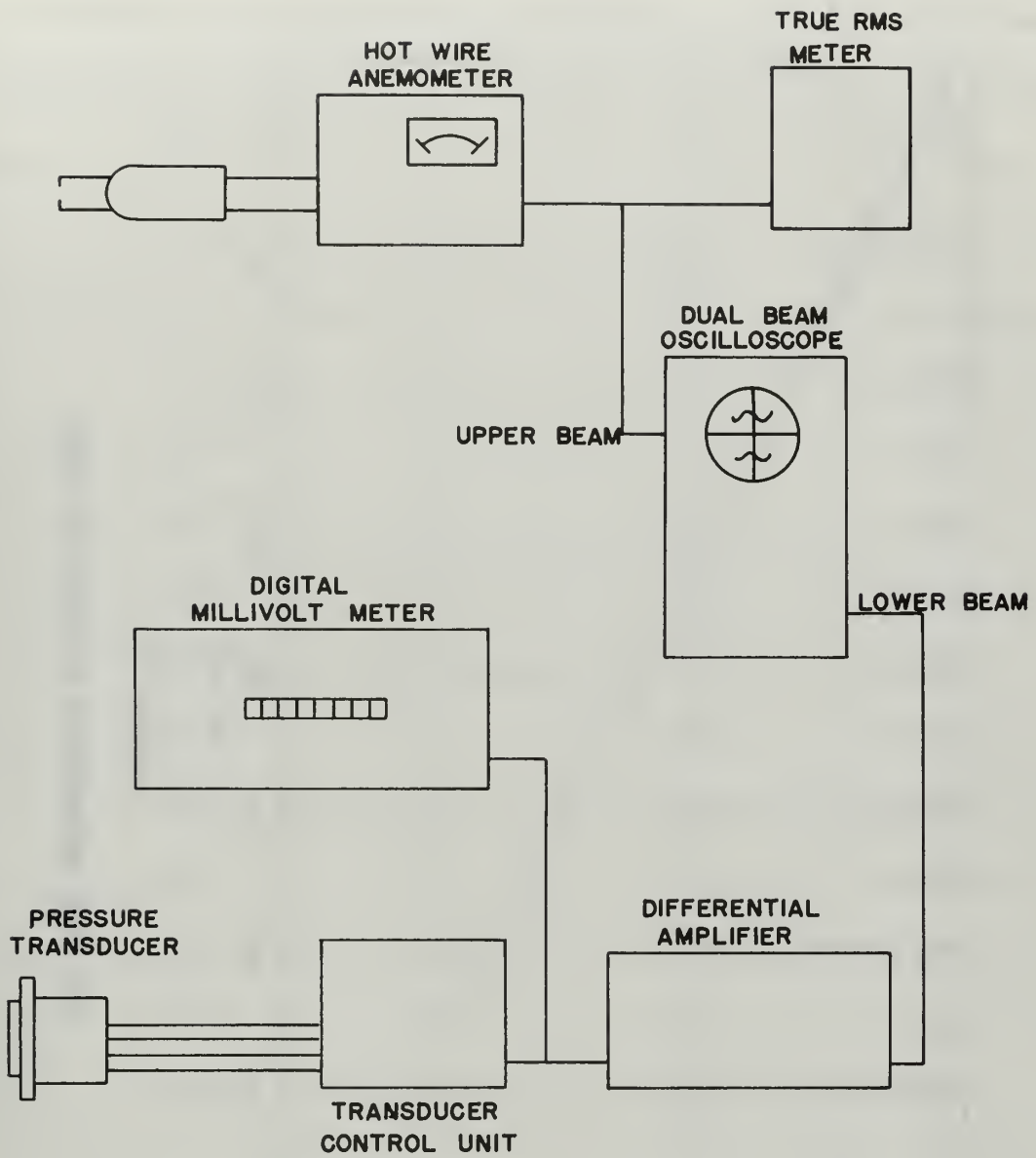


FIGURE 12

SCHEMATIC DIAGRAM OF THE INSTRUMENTATION CIRCUITRY

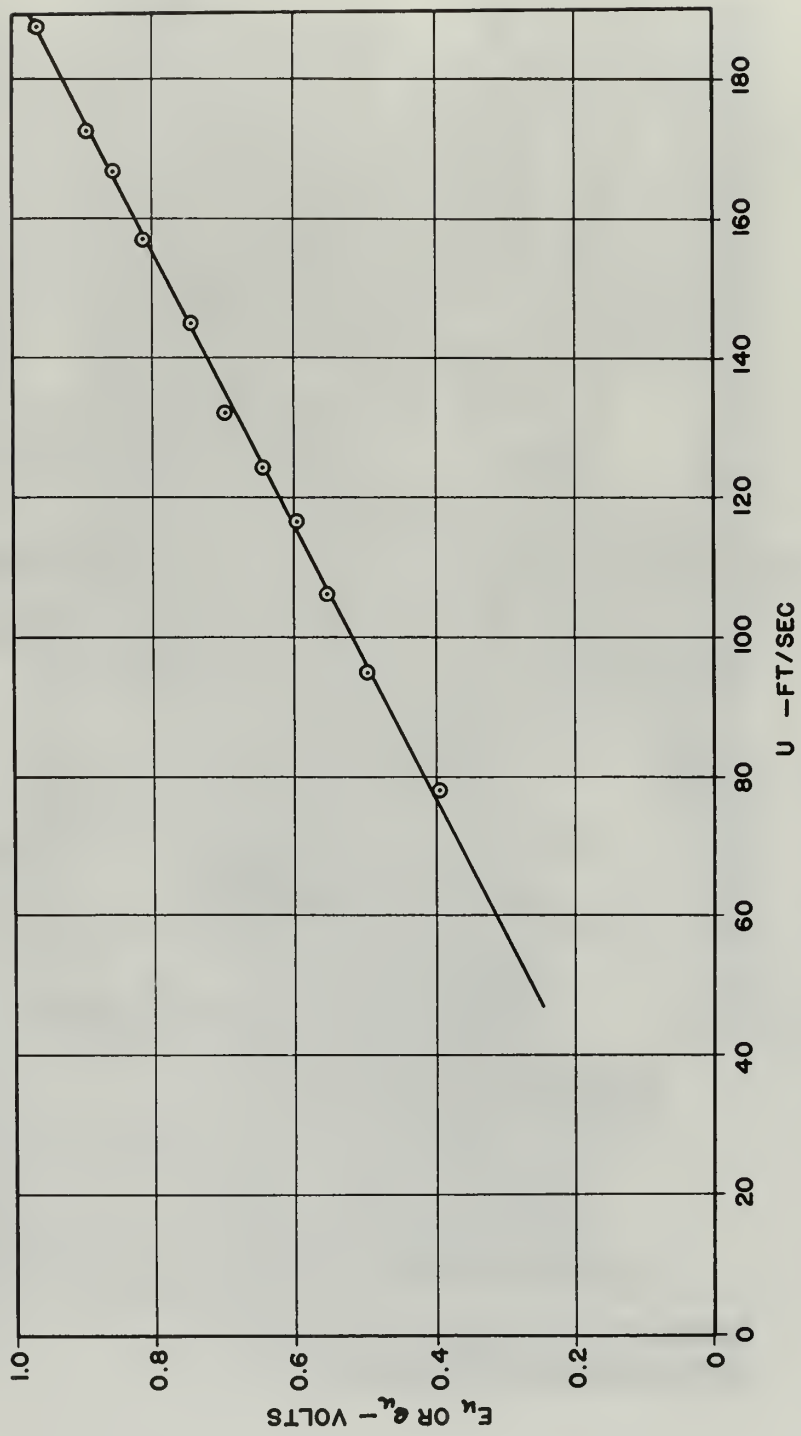


FIGURE 13

HOT WIRE ANEMOMETER CALIBRATION CURVE

Table 1

Hot Wire Anemometer Calibration and Freestream Turbulence Intensity

U_{∞}	E_u	E_u	$\frac{\bar{E}_u}{E_u} = \frac{\bar{U}}{U_{\infty}}$
ft./sec.	V. D. C.	m. V. (RMS)	Percent
78.2	0.39	1.34	0.343
95.2	0.49	1.73	0.353
106.3	0.55	2.20	0.400
116.7	0.59	2.42	0.410
124.8	0.64	2.52	0.394
132.2	0.69	2.85	0.413
145.2	0.74	3.40	0.459
157.2	0.81	3.16	0.390
167.0	0.85	3.40	0.400
172.9	0.89	3.78	0.425
188.0	0.96	4.64	0.484

each run.

For the pressure measurement runs in an oscillating flow, the test section mean velocity was set with the rotating shutter valve operating. The Reynolds number for nonsteady flows is based on the mean freestream velocity. An effort was made to obtain a sinusoidal variation of the freestream velocity. This was not possible for some of the combinations of oscillation frequencies

and velocities in the ranges covered in the present work. At certain combinations of the above parameters the velocity traces were skewed sine curves, while at other combinations one peak of the velocity trace was flattened. Only a limited amount of data was taken in the ranges where these distorted velocity traces appeared.

Table 2 contains a listing of the experimental operating conditions for each of the pressure measurement runs.

Pressure readings were recorded at various angular positions over the upper 180 degrees of the cylinder surface, starting from the forward stagnation point. The angular increment between each measurement was smaller in the regions of rapidly changing pressure. The data recording consisted of recording the mean pressure indicated by the millivolt meter and of photographing the oscilloscope velocity and pressure traces.

3. Experimental Results and Discussion.

Figure 14 shows the results of the steady flow pressure distribution measurements over the Reynolds number range from 1.95×10^5 to 3.52×10^5 . The pressure distributions measured during the present work are plotted in the usual manner of the nondimensional pressure coefficient, C_p , against θ , where θ is the angular position of a point on the cylinder surface measured from the forward stagnation point. As seen in Figure 14 the measured pressure distributions are similar to previously reported steady flow results. [1, 2, 3]

The mean pressure distributions during the nonsteady flow pressure measurement runs were obtained from the direct current component of the transducer output. Figure 15 shows the mean pressure distributions for a

Table 2

Experimental Operating Conditions

Run	$N_{Re} \times 10^{-5}$	f cycles/sec.	N_{ua}
1	1.95	0	---
2	2.45	0	---
3	3.23	0	---
4	3.43	0	---
5	3.52	0	---
6	1.95	2.0	0.118
7	1.95	29.0	0.105
8	2.45	2.0	0.208
9	2.45	12.4	0.196
10	2.45	15.0	0.221
11	2.45	18.0	0.210
12	2.45	37.0	0.169
13	2.45	53.0	0.172
14	2.45	90.0	---
15	3.23	2.0	0.408
16	3.23	3.4	0.400
17	3.23	12.2	0.387
18	3.23	29.0	0.390
19	3.43	2.0	0.378
20	3.43	7.3	0.367
21	3.52	2.0	0.405
22	3.52	12.4	---

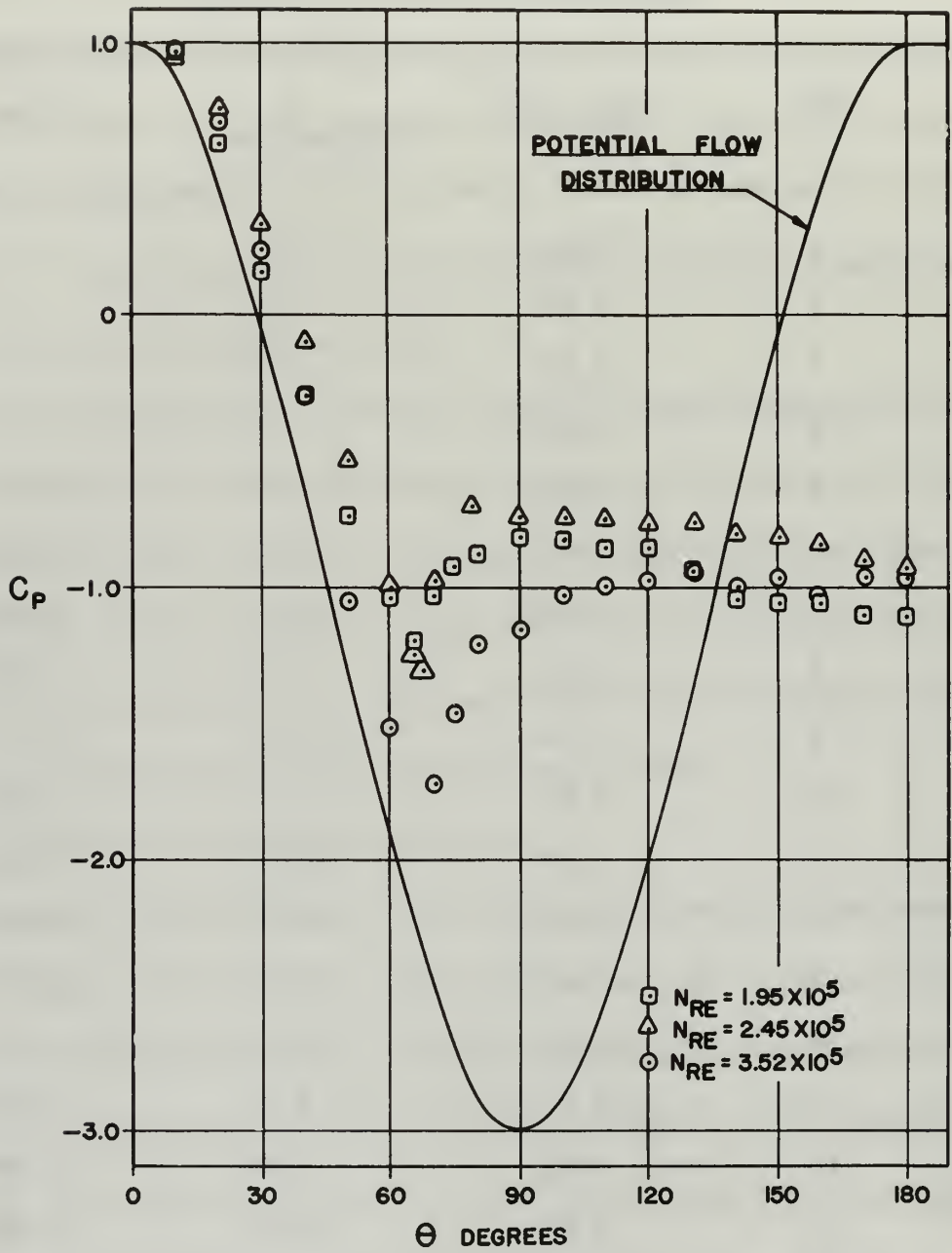


FIGURE 14

STEADY FLOW SURFACE PRESSURE DISTRIBUTION

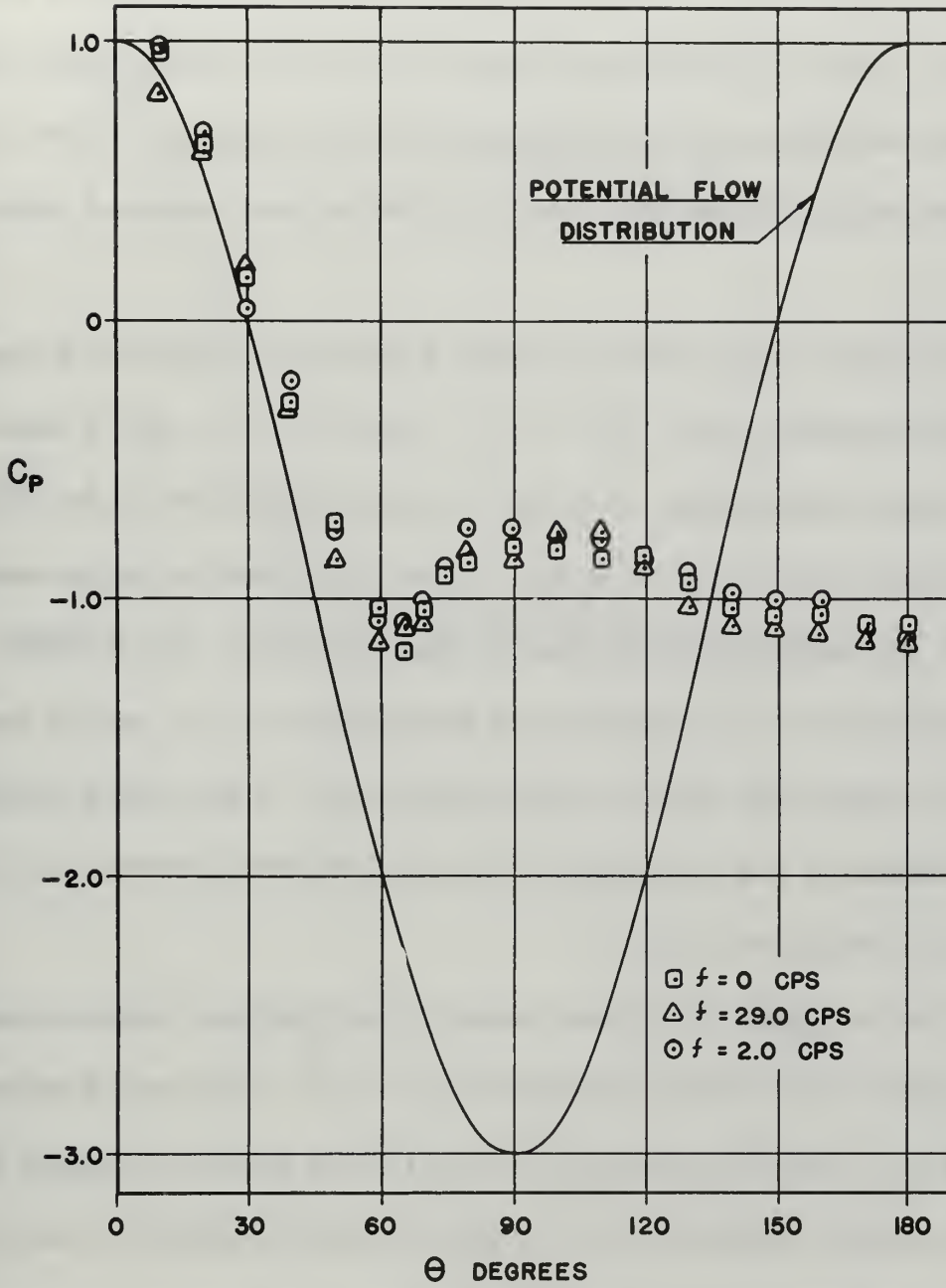


FIGURE 15

MEAN SURFACE PRESSURE
 DISTRIBUTION $N_{RE} = 1.95 \times 10^5$

freestream Reynolds number of 1.95×10^5 and oscillation frequencies of 2.0 and 29.0 cycles per second. The steady flow pressure distribution is shown for comparison. The oscillating flow is seen to have very little effect on the mean pressure distribution at this subcritical Reynolds number. Further increases in the oscillation frequency did not alter the mean pressure distribution.

The frequency range of from 2.0 to 90.0 cycles per second was investigated for the Reynolds number 2.45×10^5 . Figures 16, 17, and 18 show the mean pressure distributions measured at this low transcritical Reynolds number. In these figures it is seen that, as with the lower Reynolds number (1.95×10^5), the effects of the oscillating flow are small. The minimum pressure coefficients for the distributions measured at 15, 37, and 53 cycles per second are lower than those at other frequencies. It was found that the freestream turbulence was higher during the pressure measurement runs for 15, 37, and 53 cycles per second.

Significant changes in the mean pressure distributions become apparent as the Reynolds number is increased above 3.0×10^5 . The mean pressure distributions for a Reynolds number of 3.23×10^5 are plotted in Figures 19 and 20. The greatest departure from the steady flow distribution occurs at an oscillation frequency of 2.0 cycles per second. The minimum pressure coefficient at this frequency is 50 percent lower than the steady flow value. The region of maximum negative pressure is seen to extend over a large section of the cylinder surface at this frequency. The 2.0 cycle per second pressure distribution is quite similar to that of a steady supercritical

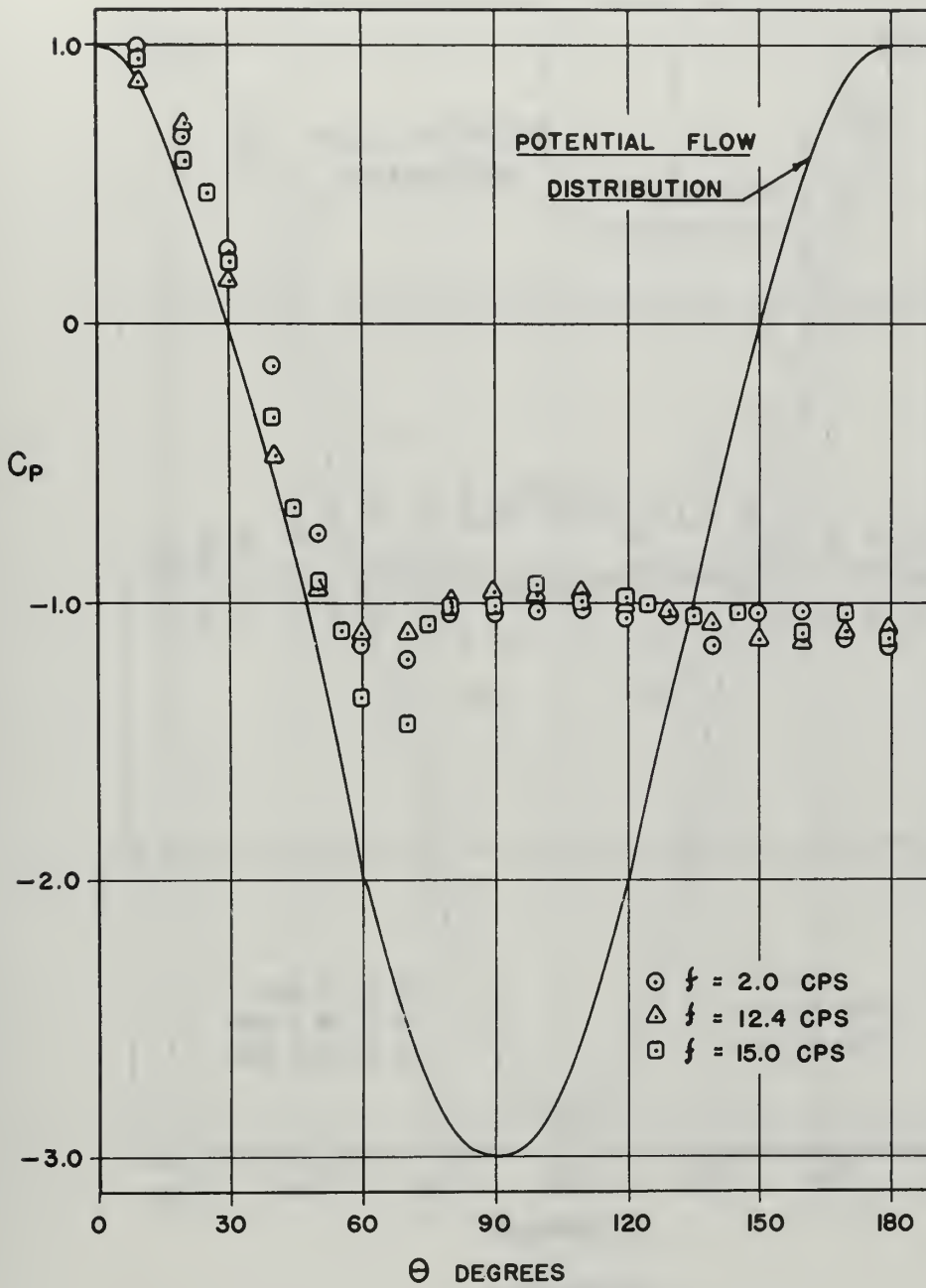


FIGURE 16

MEAN SURFACE PRESSURE
 DISTRIBUTION $N_{RE} = 2.45 \times 10^5$

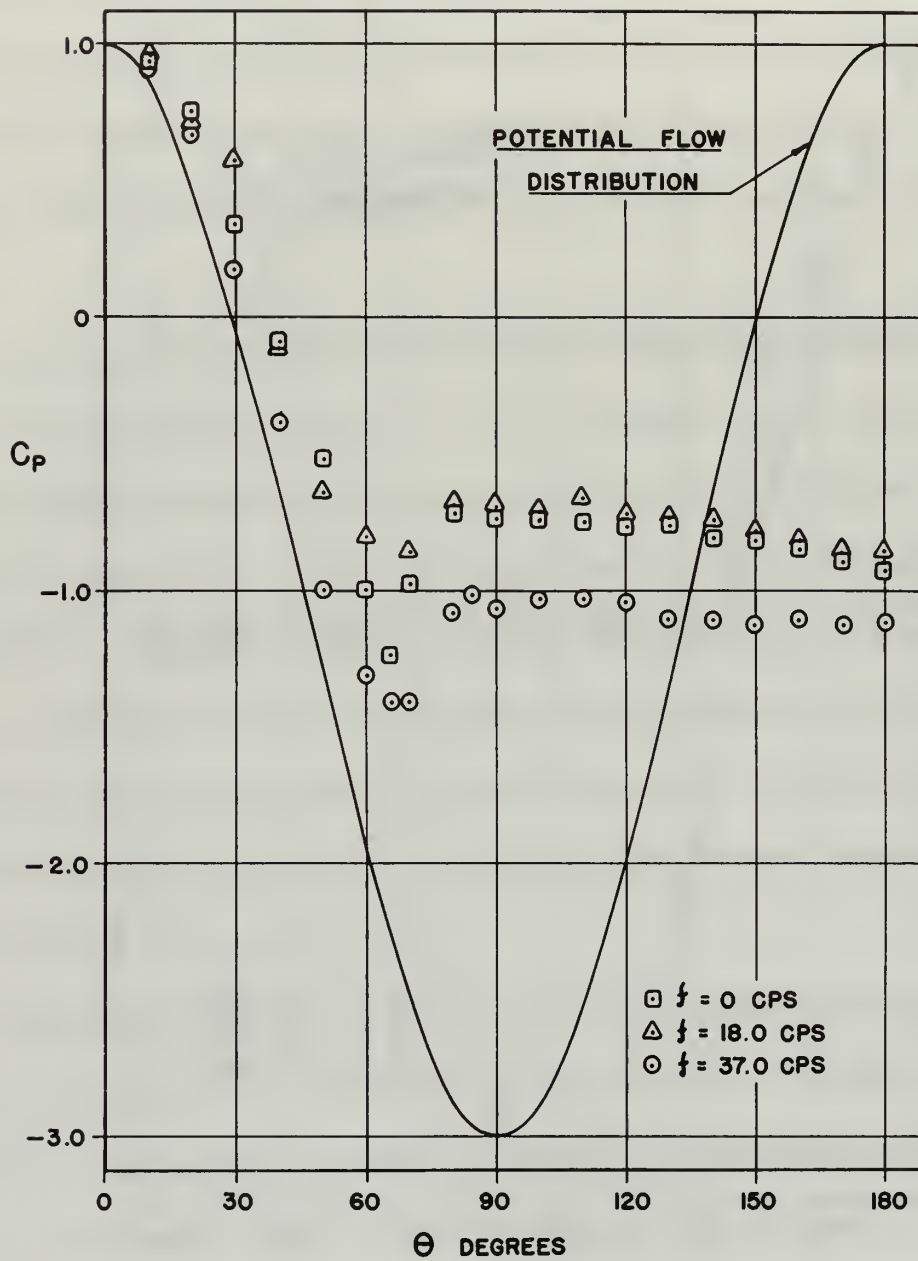


FIGURE 17

MEAN SURFACE PRESSURE
 DISTRIBUTION $N_{RE} = 2.45 \times 10^5$

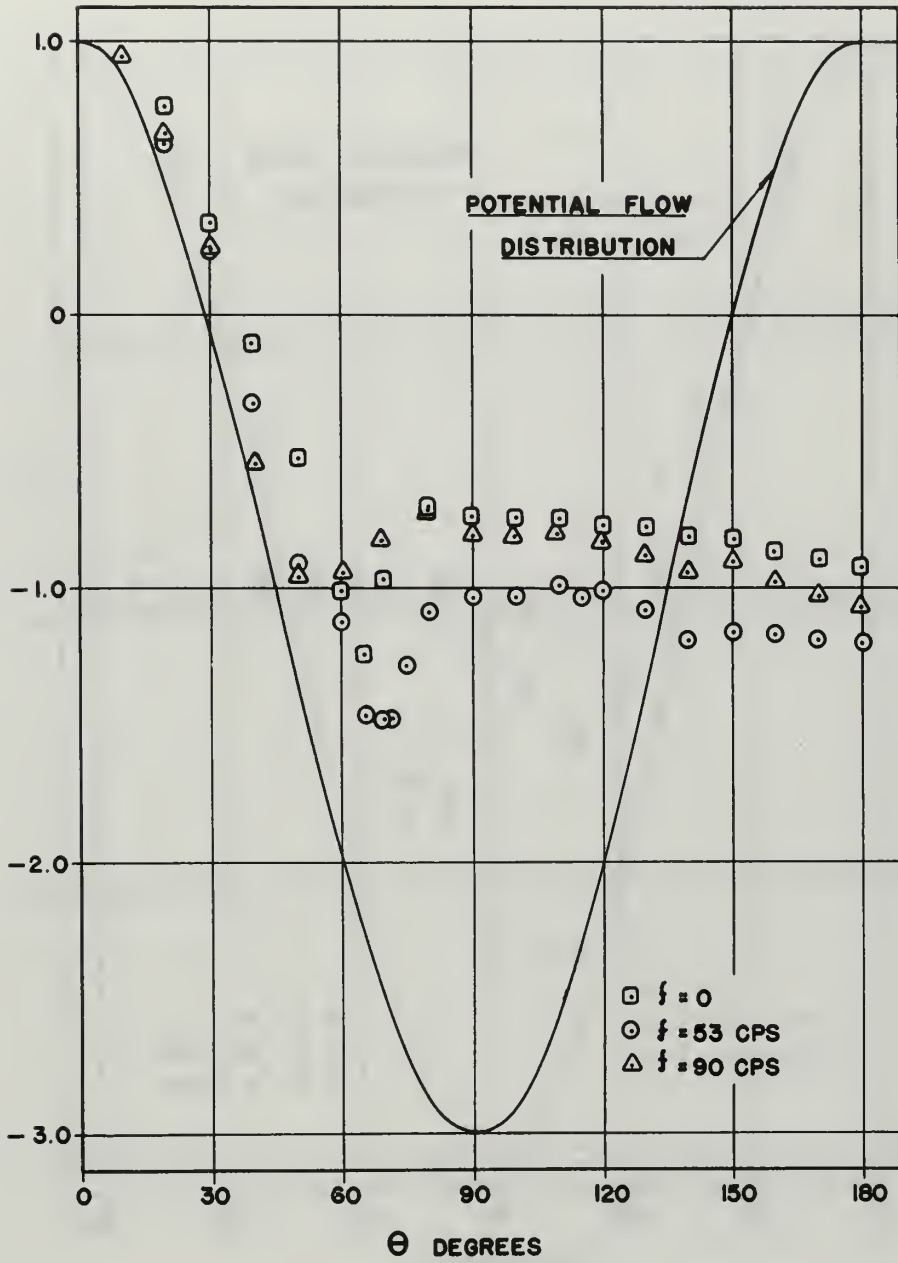


FIGURE 18

MEAN SURFACE PRESSURE
 DISTRIBUTION $N_{RE} = 2.45 \times 10^5$

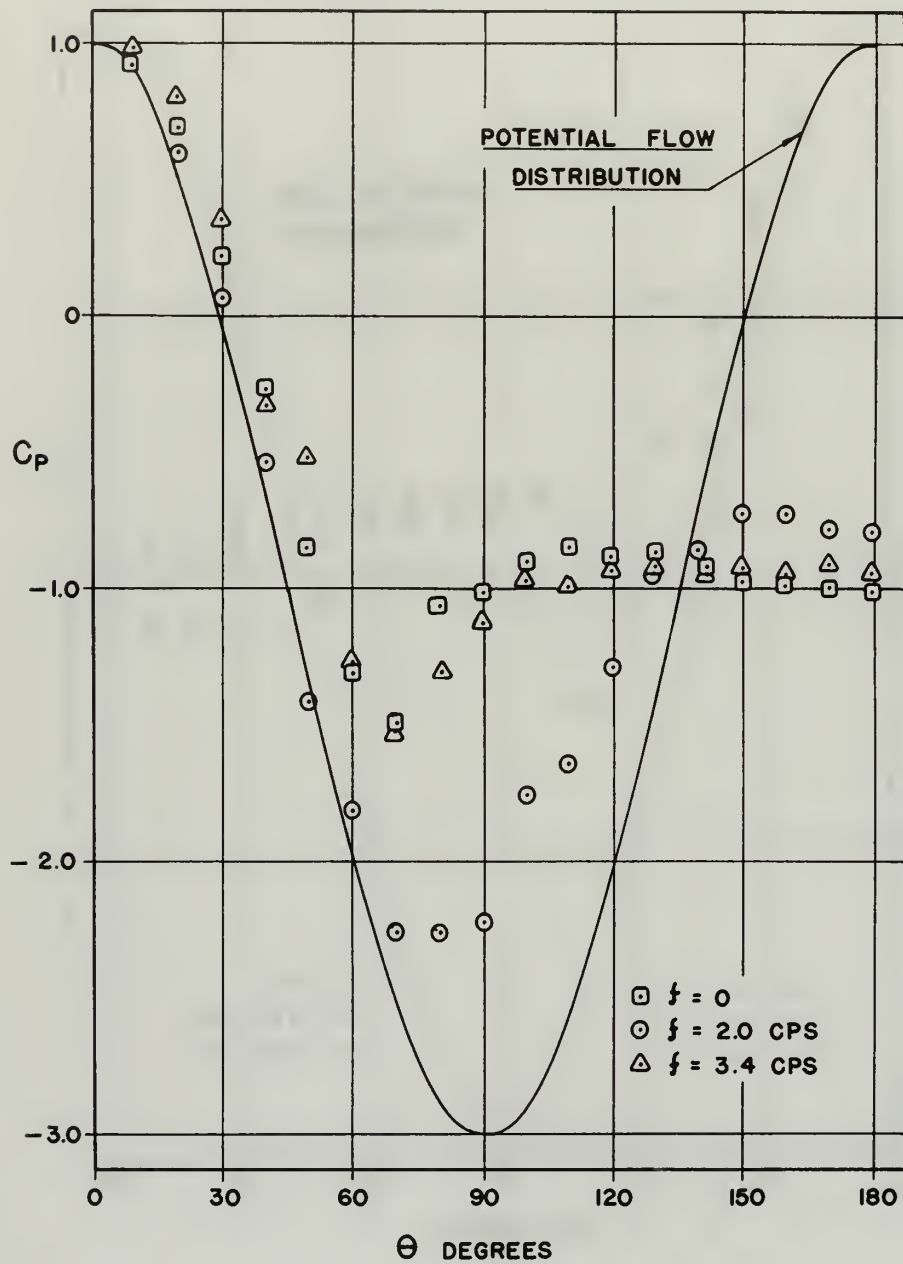


FIGURE 19

MEAN SURFACE PRESSURE
DISTRIBUTION $N_{RE} = 323 \times 10^5$

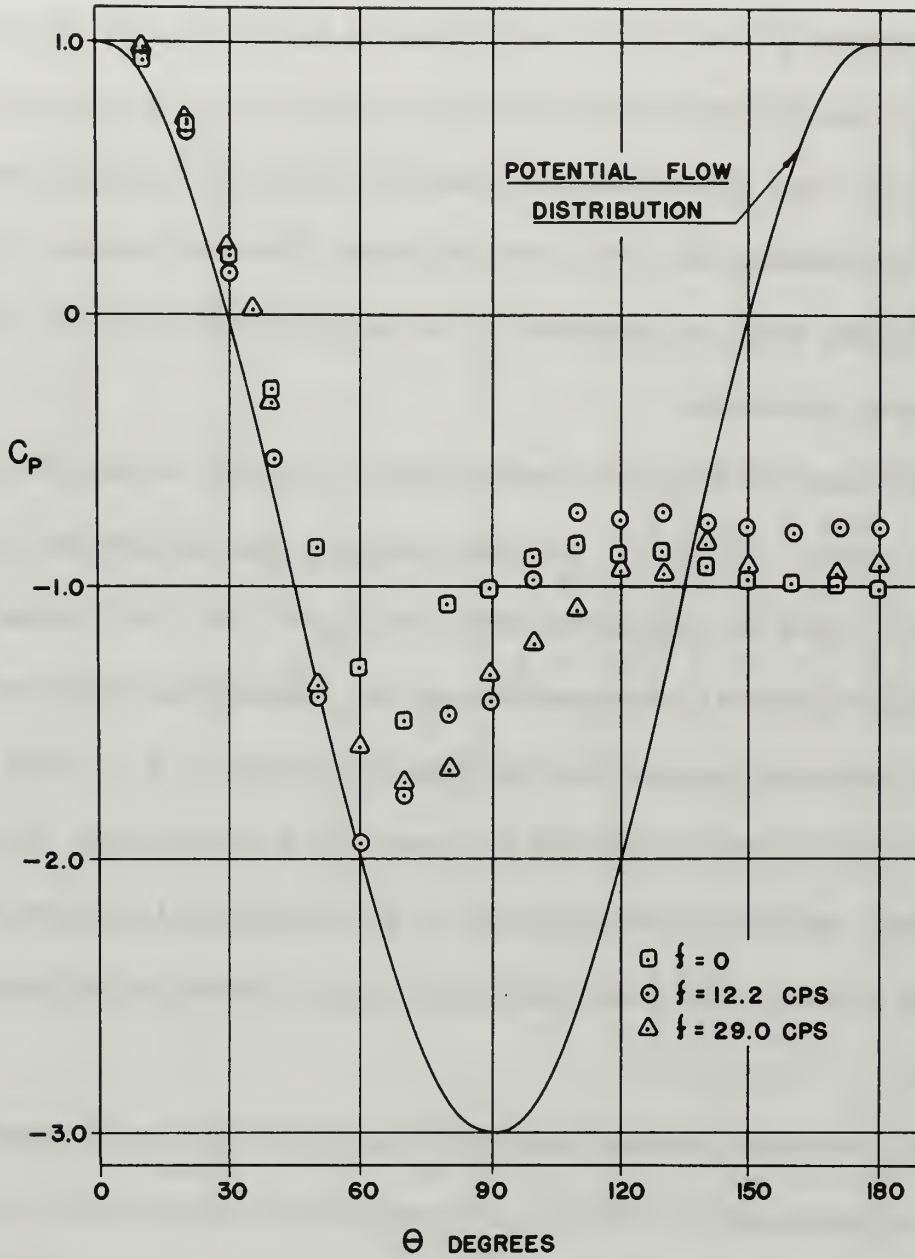


FIGURE 20

MEAN SURFACE PRESSURE
 DISTRIBUTION $N_{RE} = 3.23 \times 10^5$

Reynolds number flow. This would indicate that the effect of the oscillating flow may simply be a reduction of the critical Reynolds number. However, as the frequency of the velocity oscillation is increased, the mean pressure distribution tends toward the steady flow distribution as shown in the plots for 3.4, 12.2, and 29.0 cycles per second. All of the minimum nonsteady pressure coefficients are lower than the steady flow coefficients. This is the same effect which is observed with a steady stream when the freestream turbulence is increased.

Increasing the Reynolds number above 3.4×10^5 verified the results discussed above. Figure 21, the mean pressure distributions for $N_{Re} = 3.43 \times 10^5$, and Figure 22, the distributions for $N_{Re} = 3.52 \times 10^5$, show that as the Reynolds number is increased through the transcritical range the minimum pressure coefficient approaches the theoretical value of -3.0. This is the normal Reynolds number effect on the steady flow distribution. The nonsteady flow effects, again are most apparent for an oscillation frequency of 2.0 cycles per second, with a reduction of frequency effect as the frequency is increased.

From the mean pressure plots it is seen that below a Reynolds number value of approximately 3.0×10^5 , the oscillating flow has very little, if any, effect on the mean pressure distribution. The oscillating flow effects are most pronounced at a frequency of 2.0 cycles per second and in the Reynolds number range above 3.0×10^5 . At frequencies higher than 2.0 cps, the pressure distribution about the cylinder is essentially the same as that measured in a highly turbulent freestream. However, in the present work the

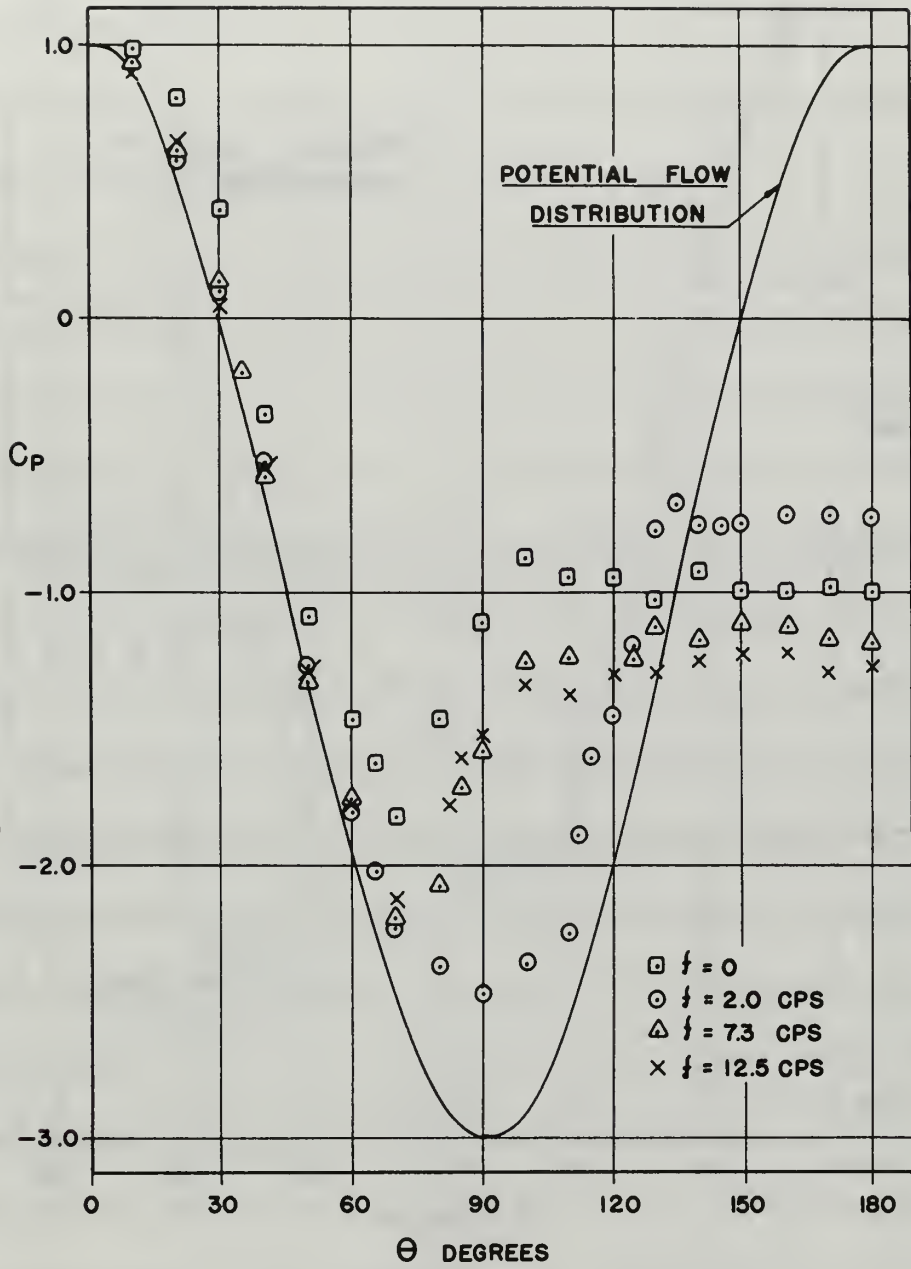


FIGURE 21

MEAN SURFACE PRESSURE
 DISTRIBUTION $N_{RE} = 3.43 \times 10^5$

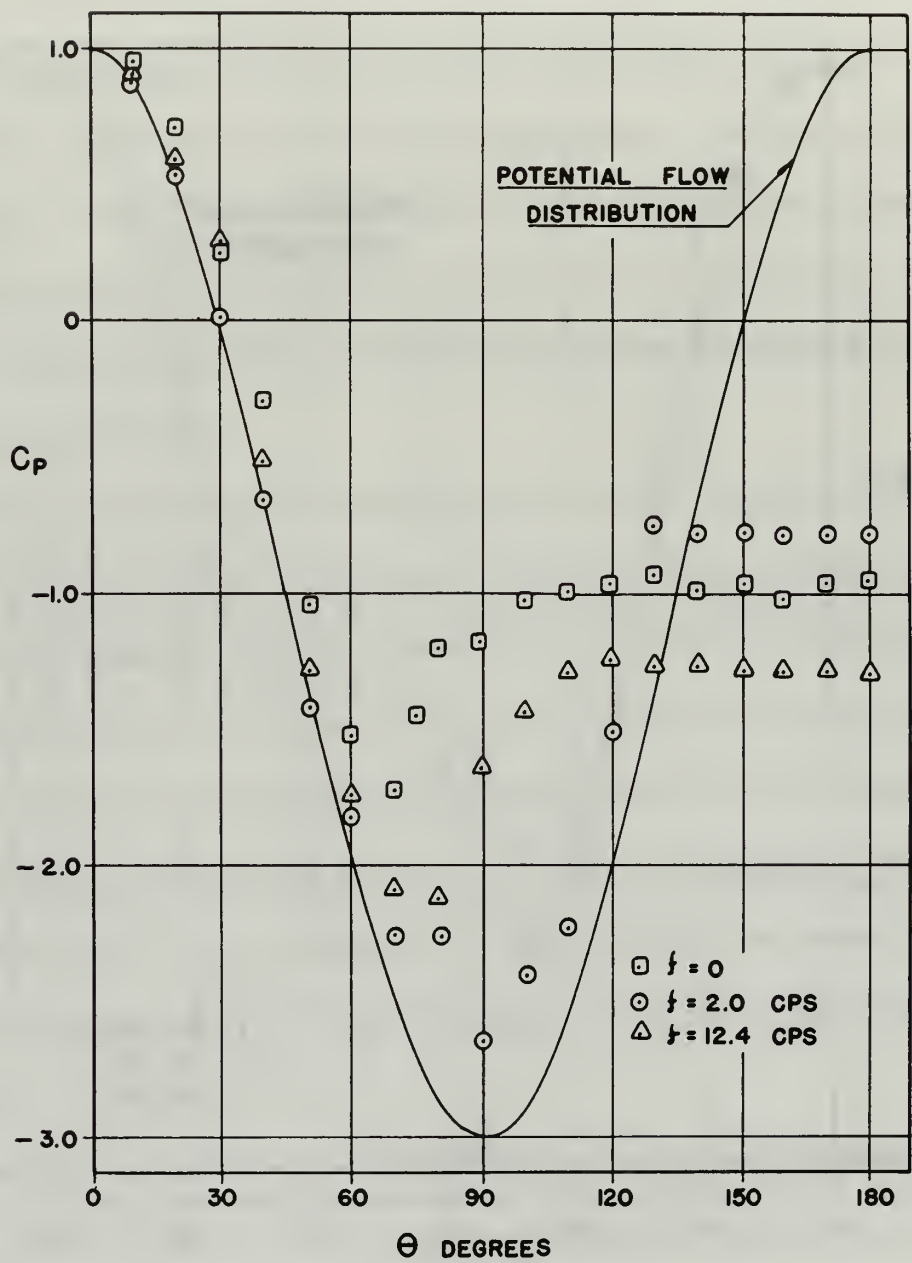


FIGURE 22

MEAN SURFACE PRESSURE
 DISTRIBUTION $N_{RE} = 3.52 \times 10^5$

velocity disturbance amplitude was in the range of from 10.5 to 40.6 percent of the mean freestream velocity, well above the usual range of freestream turbulence intensities.

The instantaneous pressure variations, which were recorded photographically, reveal several interesting phenomena.

Figure 23 shows the freestream velocity and surface pressure traces for a Reynolds number value of 1.95×10^5 and an oscillation frequency of 2.0 cycles per second. The upper trace is the freestream velocity. (In all the oscilloscope photographs shown the velocity traces are inverted due to the coupling in the hot wire anemometer circuit.) At the forward stagnation point ($\theta = 0^\circ$) it is seen that the total pressure decreases as the velocity increases. Also the maximum pressure fluctuation amplitude occurs at this point. Downstream of the forward stagnation point the pressure amplitude decreases until the point of minimum mean pressure coefficient is reached. Aft of this location on the cylinder surface the pressure fluctuation amplitude remains constant. (The signal to noise ratio on the pressure traces at the forward stagnation point is approximately seven to one, while at the rear stagnation point it is between three and four to one.)

Another effect of the oscillating flow is seen in Figure 23. An angular phase shift between the freestream velocity fluctuation and the cylinder surface pressure fluctuation develops. The change in the pressure and hence the velocity in the boundary layer begins to lag the change of the freestream velocity. This indicates that the pressure gradient, which is necessary to change the velocity of the stream, is not seen in the boundary layer as it is

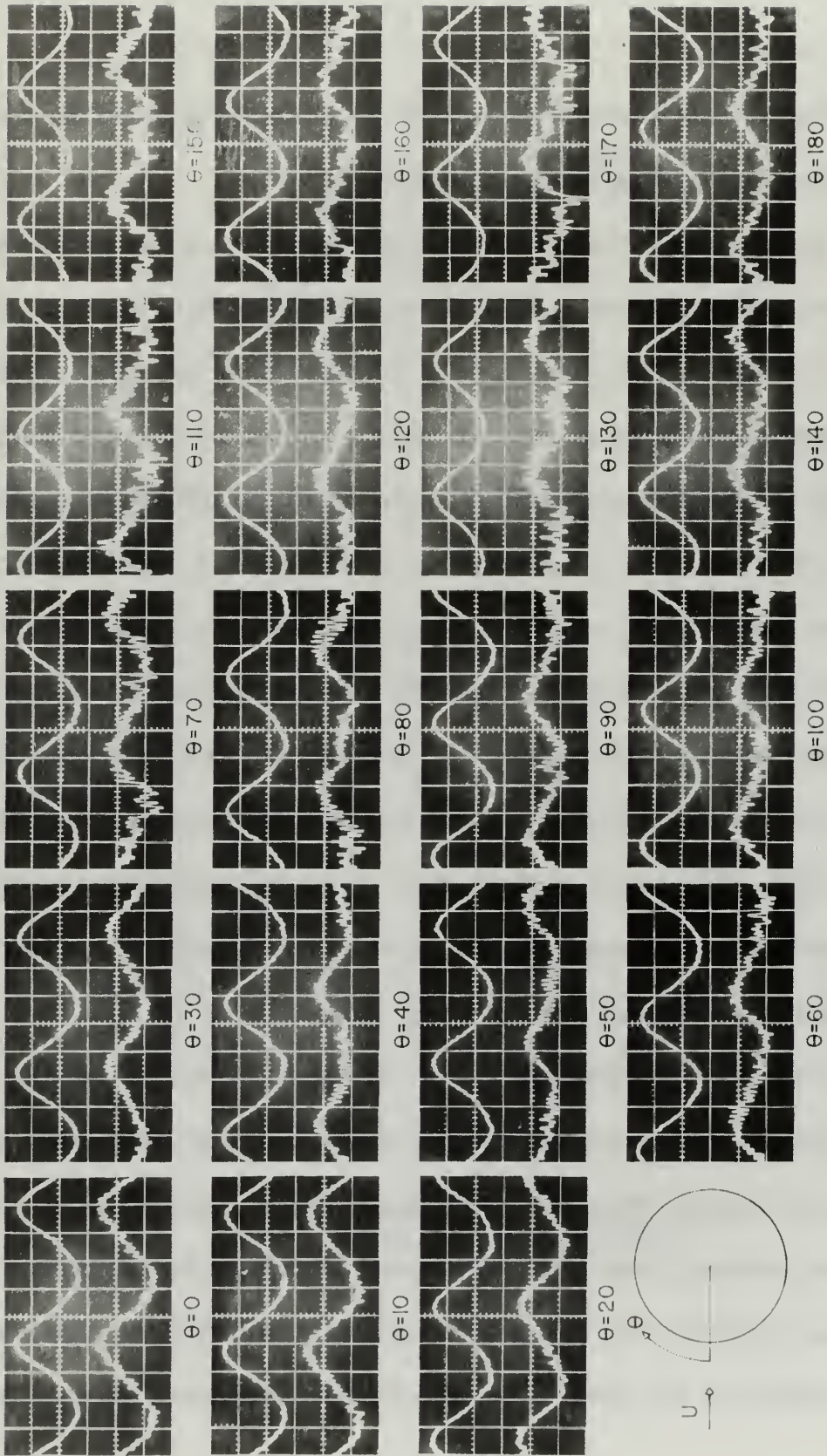


FIGURE 23
 OSCILLOSCOPE TRACES OF THE FREE STREAM VELOCITY AND
 CYLINDER SURFACE PRESSURE $N_{RE} = 1.95 \times 10^5$ $f = 2.0$ cps

seen in the freestream. This result is contrary to Lighthill's theory which predicts that the velocity changes in the boundary layer will lead the changes of the freestream velocity. [15] However, Lighthill's calculations are based on the assumption that the velocity fluctuations are small compared to the freestream velocity. Although Hori reports observing a phase shift, he does not specify whether it was a lead or a lag. His experiment was conducted at $N_{Re} = 9,000$ with an oscillation frequency of 1.1 cycles per second. Hori indicates that the phase shift is 'small' upstream of the point of minimum pressure and 'very large' near the boundary layer separation point. In the present work the phase difference is clearly evidenced in the photographs of Figure 23 as far forward as $\theta = 20$ degrees. Hori measured the magnitude of the velocity phase difference to be 45 degrees at a point within 0.5 mm of the surface at $\theta = 75$ degrees. The phase shift for the conditions shown in Figure 23 was 60 degrees. The sweep delay line in the dual-beam oscilloscope was used for this measurement.

A close inspection of the photographs of Figure 23 shows that between the angular positions of 30 and 40 degrees the lower portion of the pressure trace does not peak as before. The pressure trace for 40 degrees shows small disturbances (above the noise level) in the low pressure area, while at 50 degrees these disturbances are seen over most of the oscillation cycle. This may indicate the transition from a laminar to a turbulent boundary layer over part of the cycle, thus movement of the transition point. At 60 degrees there is an indication of an instantaneous pressure increase in the low pressure portion of the cycle, which becomes more pronounced at 70 to 80 degrees.

The cause of this pressure increase may be the separation of the boundary layer. The pressure traces from the 90 degree position to the rear stagnation point are all quite similar and probably indicate a stable wake condition. If the above assumptions are correct, this would indicate that even though the effects of the oscillating flow are not evident in the mean pressure distribution for this subcritical Reynolds number, they do influence the boundary layer formation and separation.

Figure 24 shows the freestream velocity and surface pressure traces for $N_{Re} = 3.52 \times 10^5$ at an oscillation frequency of 12.4 cycles per second. In this set of photographs a phase lag between the pressure and velocity traces appears at the forward stagnation point. This was most probably caused by an instrumentation lag in the transducer and associated circuitry since the magnitude of this initial phase difference increased with frequency. At this higher frequency and Reynolds number the flattening of the pressure trace, which was seen at the 40 degree position in Figure 23, is apparent at the forward stagnation point. This occurs even though the velocity profile is smooth. In Figure 24 this flattening of the pressure trace becomes broader as the angular position is increased. This indicates that a flow disturbance in the boundary layer is present over more and more of the oscillation cycle. At 60 degrees this disturbance is present over the entire cycle. If the assumptions postulated above are correct, this would indicate that the boundary layer flow, even at the forward stagnation point becomes turbulent when the freestream velocity has reached a maximum and begins to decelerate. The photograph of the pressure trace for the 70 degree position shows that

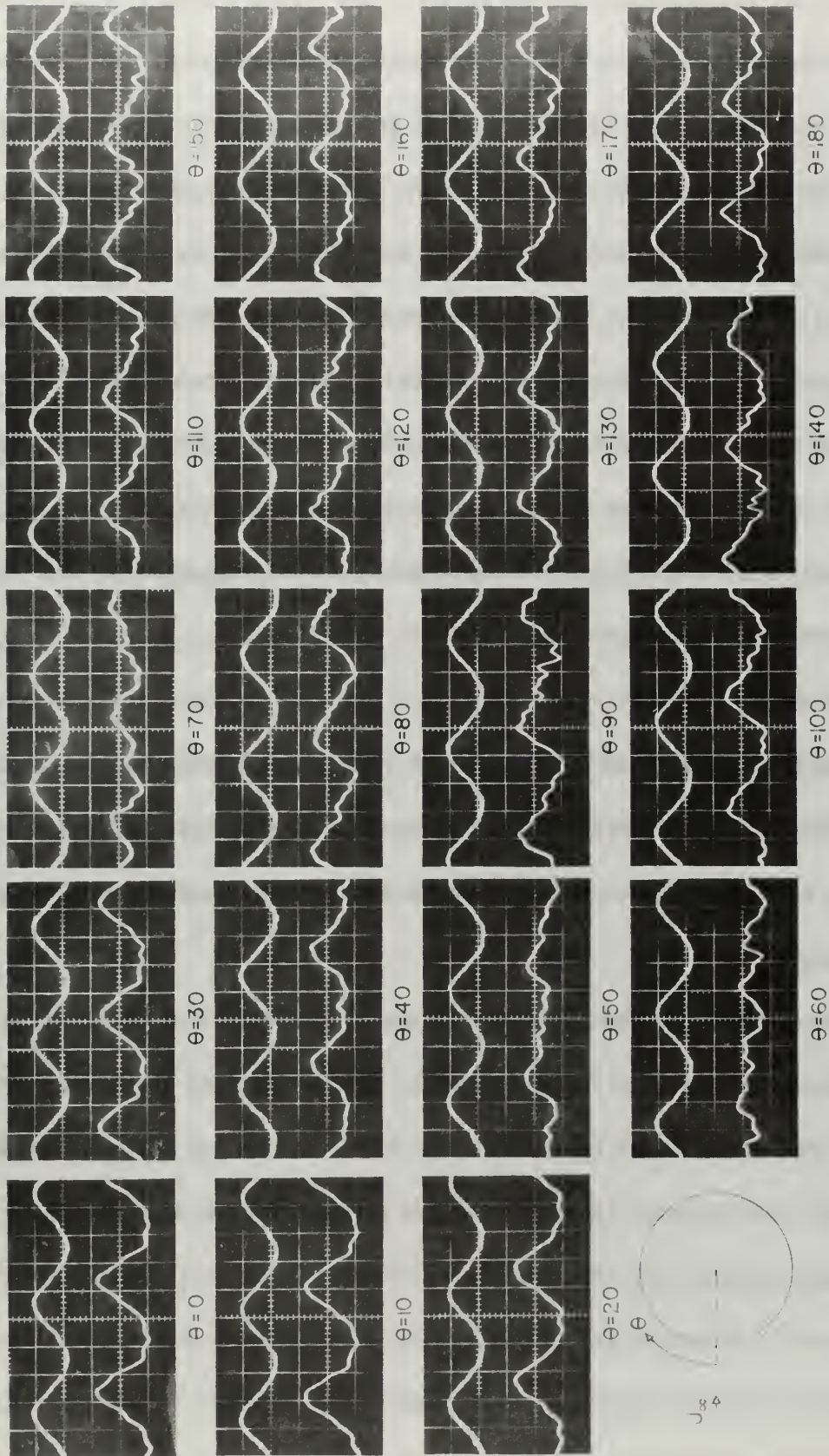


FIGURE 24
 OSCILLOSCOPE TRACES OF THE FREE STREAM VELOCITY AND
 CYLINDER SURFACE PRESSURE $N_{RE} = 3.52 \times 10^5$ $f = 12.4$ cps

the maximum pressure occurs at the point in the cycle which corresponds to the point of maximum velocity. All the photographs from the 80 degree position to the rear stagnation point show that the pressure oscillation is again back in phase with the freestream velocity. Moreover in this region the pressure traces are all similar which may be taken as an indication of a stable wake. Therefore the boundary layer separation point must be upstream of the 80 degree position during the complete cycle. The results shown in Figure 24 are typical of the results obtained over the entire Reynolds number range of the present work at all the frequencies above 10 cycles per second. Note that the phase shift, which developed at lower frequencies, did not occur at the higher frequencies.

4. Conclusions.

The effects of nonsteady flow on the pressure distribution about a circular cylinder depend principally on the frequency of the freestream velocity oscillations and on the Reynolds number which is based on the mean free-stream velocity.

The mean pressure distributions in the subcritical and low transcritical Reynolds number ranges are not affected by the oscillating flow over the oscillation frequency range of from 2.0 to 90.0 cycles per second. In the mid and high transcritical Reynolds number ranges (above approximately 3×10^5) the mean pressure distributions are affected most by low frequency flow oscillations of 2.0 cycles per second. The mean pressure distributions measured in this range indicate a reduction of the critical Reynolds number. An increase of the frequency shifts the pressure distribution back toward the

steady flow distribution.

An angular phase shift between the oscillations of the freestream velocity and the surface pressure develops between the forward stagnation point and the point of minimum mean pressure at an oscillation frequency of 2.0 cycles per second. This phase shift occurs over the entire Reynolds number range of the present work. The phase shift shows that the oscillation of the velocity in the boundary layer lags the oscillation of the freestream. This effect of the nonsteady flow was not observed at oscillation frequencies of 10 cycles per second and above.

An investigation to determine the nature of the flow in the boundary layer about a circular cylinder in a nonsteady stream should be conducted. Hot wire anemometer surveys of the nonsteady boundary layer would answer many of the questions posed by the present work. The experimental facilities soon to be available at the Naval Postgraduate School should be ideal for conducting these studies.

ACKNOWLEDGEMENT

The author wishes to express his indebtedness to Dr. James A. Miller, Associate Professor, Department of Aeronautics, for his encouragement and guidance during the present work.

Grateful acknowledgement is also due Dr. Louis V. Schmidt for his many helpful suggestions.

BIBLIOGRAPHY

1. Schlichting, H. Boundary Layer Theory, 4th ed. Pergamon Press, 1955.
2. Fage, A. The air flow around a circular cylinder in the region where the boundary layer separates from the surface. British A. R. C., R. and M. 1179, August, 1928.
3. Fage, A. and Falkner, V. M. Further experiments on the flow about a circular cylinder. British A. R. C., R. and M. 1369, February, 1931.
4. Fage, A. and Falkner, V. M. The drag of circular cylinders and spheres at high values of Reynolds number. British A. R. C., R. and M. 1370, May, 1930.
5. Gerrard, J. H. A disturbance-sensitive Reynolds number range of flow past a circular cylinder. Journal of Fluid Mechanics, v. 22, Part 1, May, 1965.
6. Schmidt, L. V. Measurement of fluctuating air loads on a circular cylinder. California Institute of Technology, PhD. Thesis, 1963.
7. Spitzer, R. E. Measurements of unsteady pressures and wave fluctuations for flow over a cylinder at supercritical Reynolds number. California Institute of Technology, Aeronautical Engineer Degree Thesis, 1965.
8. Glauert, M. B. The laminar boundary layer on oscillating plates and cylinders. Journal of Fluid Mechanics, v. 1, Part 1, May, 1956.
9. Hori, E. Experiments on the boundary layer of an oscillating circular cylinder. Bulletin of the Japan Society of Mechanical Engineers, v. 6, no. 22, 1963.
10. Vidal, R. J. Research on rotating stall in axial flow compressors. Cornell Aeronautical Laboratory, Inc. W. A. D. C. Technical Report 59-75, Part III, January 1959.
11. Nickerson, R. J. The effect of freestream oscillations on the laminar boundary layers on a flat plate. Massachusetts Institute of Technology, PhD. Thesis, 1957.
12. Feiler, C. E. and Yeager, E. B. Effect of large-amplitude oscillations on heat-transfer. N. A. S. A., T. R. R-142, 1962.

13. Feiler, C. E. Experimental heat-transfer and boundary-layer behavior with 100-cps flow oscillations. N. A. S. A., T. N. D-2521, 1964.
14. Miller, J. A. Transition in oscillating Blasius flow. Illinois Institute of Technology, PhD. Thesis, 1963.
15. Lighthill, M. J. The response of laminar skin friction and heat transfer to fluctuations in the stream velocity. Proceedings of the Royal Society, Series A, v. 224, no. 1156, June, 1954.

APPENDIX I

Experimental Data

Table 3 pages 60 thru 81

Table 3

Mean Pressure Coefficients

Run Number 1 $N_{Re} = 1.95 \times 10^5$ $f = 0$ cps

θ (degrees)	C_p (dimensionless)	θ (degrees)	C_p (dimensionless)
0	1.00	90	-0.82
10	0.96	100	-0.83
20	0.62	110	-0.86
30	0.15	120	-0.86
40	-0.30	130	-0.94
50	-0.74	140	-1.05
60	-1.04	150	-1.07
65	-1.20	160	-1.06
70	-1.03	170	-1.10
75	-0.92	180	-1.11
80	-0.88		

Table 3 (cont'd)

Run Number 2 $N_{Re} = 2.45 \times 10^5$

f = 0 cps

θ (degrees)	C_p (dimensionless)	θ (degrees)	C_p (dimensionless)
0	1.00	90	-0.74
10	0.94	100	-0.74
20	0.75	110	-0.75
30	0.33	120	-0.77
40	-0.10	130	-0.76
50	-0.53	140	-0.81
60	-1.01	150	-0.82
65	-1.25	160	-0.84
67	-1.31	170	-0.90
70	-0.97	180	-0.93
80	-0.70		

Table 3 (cont'd)

Run Number 3

 $N_{Re} = 3.23 \times 10^5$

f = 0 cps

θ	C_p	θ	C_p
(degrees)	(dimensionless)	(degrees)	(dimensionless)
0	1.00	100	-0.90
10	0.92	110	-0.85
20	0.68	120	-0.88
30	0.22	130	-0.87
40	-0.28	140	-0.93
50	-0.86	150	-0.98
60	-1.31	160	-0.99
70	-1.50	170	-1.00
80	-1.07	180	-1.01
90	-1.01		

Table 3 (cont'd)

Run Number 4 $N_{Re} = 3.43 \times 10^5$ $f = 0$ cps

θ (degrees)	C_p (dimensionless)	θ (degrees)	C_p (dimensionless)
0	1.00	97	-0.98
10	0.98	100	-0.88
20	0.79	105	-0.88
30	0.38	110	-0.96
40	-0.36	115	-0.95
45	-0.66	120	-0.96
50	-1.10	125	-1.04
60	-1.47	130	-1.04
65	-1.63	135	-1.01
70	-1.83	140	-0.93
75	-1.79	145	-0.98
80	-1.46	150	-1.00
85	-1.18	160	-1.01
90	-1.12	170	-0.99
95	-1.07	180	-1.01

Table 3 (cont'd)

Run Number 5 $N_{Re} = 3.52 \times 10^5$ $f = 0$ cps

θ (degrees)	C_p (dimensionless)	θ (degrees)	C_p (dimensionless)
0	1.00	90	-1.18
10	0.94	100	-1.03
20	0.70	110	-1.00
30	0.24	120	-0.97
40	-0.30	130	-0.94
50	-1.05	140	-1.00
60	-1.52	150	-0.97
70	-1.73	160	-1.03
75	-1.46	170	-0.97
80	-1.21	180	-0.96

Table 3 (cont'd)

Run Number 6 $N_{Re} = 1.95 \times 10^5$ $N_{ua} = 0.108$ $f = 2.0$ cps

θ (degrees)	C_p (dimensionless)	θ (degrees)	C_p (dimensionless)
0	1.00	80	-0.77
10	0.97	90	-0.75
20	0.68	100	-0.78
30	0.03	110	-0.79
40	-0.22	120	-0.87
50	-0.75	130	-0.93
60	-1.08	140	-0.98
65	-1.12	150	-1.01
67	-1.12	160	-1.04
70	-1.08	170	-1.11
75	-0.90	180	-1.16

Table 3 (cont'd)

Run Number 7 $N_{Re} = 1.95 \times 10^5$ $N_{ua} = 0.105$ $f = 29.0$ cps

θ (degrees)	C_p (dimensionless)	θ (degrees)	C_p (dimensionless)
0	1.00	100	-0.77
10	0.80	105	-0.77
20	0.62	110	-0.77
30	0.20	115	-0.80
35	-0.18	120	-0.89
40	-0.41	125	-0.84
45	-0.74	130	-1.05
50	-0.86	135	-1.08
55	-1.01	140	-1.10
60	-1.17	150	-1.10
65	-1.11	155	-1.14
70	-1.08	160	-1.14
75	-0.92	165	-1.10
80	-0.83	170	-1.17
85	-0.83	175	-1.14
90	-0.86	180	-1.17
95	-0.86		

Table 3 (cont'd)

Run Number 8 $N_{Re} = 2.45 \times 10^5$ $N_{ua} = 0.208$ $f = 2.0$ cps

θ	C_p	θ	C_p
(degrees)	(dimensionless)	(degrees)	(dimensionless)
0	1.00	100	-1.04
10	0.97	110	-1.03
20	0.67	120	-1.06
30	0.26	130	-1.04
40	-0.28	140	-1.16
50	-0.76	150	-1.04
60	-1.15	160	-1.04
70	-1.21	170	-1.14
80	-1.04	180	-1.15
90	-1.04		

Table 3 (cont'd)

Run Number 9 $N_{Re} = 2.45 \times 10^5$ $N_{ua} = 0.196$ $f = 12.4$ cps

θ (degrees)	C_p (dimensionless)	θ (degrees)	C_p (dimensionless)
0	1.00	100	-0.97
10	0.86	110	-0.98
20	0.70	120	-1.02
30	0.15	130	-1.03
40	-0.48	140	-1.10
50	-0.96	150	-1.14
60	-1.12	160	-1.14
70	-1.12	170	-1.12
80	-1.02	180	-1.12
90	-0.97		

Table 3 (cont'd)

Run Number 10 $N_{Re} = 2.45 \times 10^5$ $N_{ua} = 0.221$ $f = 15.0$ cps

θ (degrees)	C_p (dimensionless)	θ (degrees)	C_p (dimensionless)
0	1.00	90	-1.03
10	0.94	95	-1.02
20	0.54	100	-1.02
25	0.46	105	-0.98
30	0.22	110	-1.00
35	-0.06	115	-1.00
40	-0.34	120	-1.00
45	-0.67	125	-1.01
50	-0.91	130	-1.04
55	-1.10	135	-1.05
60	-1.36	140	-1.10
65	-1.43	145	-1.04
70	-1.44	150	-1.09
75	-1.39	160	-1.12
80	-1.40	170	-1.05
85	-1.07	180	-1.14

Table 3 (cont'd)

Run Number 11 $N_{Re} = 2.45 \times 10^5$ $N_{ua} = 0.210$ $f = 18.0$ cps

θ (degrees)	C_p (dimensionless)	θ (degrees)	C_p (dimensionless)
0	1.00	100	-0.71
10	0.93	110	-0.67
20	0.71	120	-0.72
30	0.58	130	-0.73
40	-0.10	140	-0.75
50	-0.65	150	-0.78
60	-0.81	160	-0.82
70	-0.85	170	-0.85
80	-0.69	180	-0.85
90	-0.69		

Table 3 (cont'd)

Run Number 12 $N_{Re} = 2.45 \times 10^5$ $N_{ua} = 0.169$ $f = 37.0$ cps

θ	C_p	θ	C_p
(degrees)	(dimensionless)	(degrees)	(dimensionless)
0	1.00	90	-1.07
10	0.92	95	-1.10
20	0.63	100	-1.03
30	0.17	105	-1.04
35	-0.08	110	-1.03
40	-0.39	115	-1.06
45	-0.70	120	-1.05
50	-1.01	125	-1.09
55	-1.25	130	-1.11
60	-1.31	135	-1.12
65	-1.42	140	-1.14
70	-1.41	150	-1.16
73	-1.33	160	-1.14
75	-1.23	170	-1.16
80	-1.08	180	-1.19
85	-1.00		

Table 3 (cont'd)

Run Number 13 $N_{Re} = 2.45 \times 10^5$ $N_{ua} = 0.172$ $f = 53.0$ cps

θ (degrees)	C_p (dimensionless)	θ (degrees)	C_p (dimensionless)
0	1.00	90	-1.05
10	0.91	95	-1.07
20	0.62	100	-1.04
30	0.24	105	-1.05
35	-0.07	110	-1.00
40	-0.33	115	-1.04
45	-0.60	120	-1.01
50	-0.91	125	-1.05
55	-1.15	130	-1.09
60	-1.14	135	-1.15
65	-1.47	140	-1.19
70	-1.48	145	-1.21
72	-1.48	150	-1.18
75	-1.29	160	-1.18
80	-1.09	170	-1.19
85	-1.05	180	-1.21

Table 3 (cont'd)

Run Number 14 $N_{Re} = 2.45 \times 10^5$ $N_{ua} = \text{---}$ $f = 90.0 \text{ cps}$

θ (degrees)	C_p (dimensionless)	θ (degrees)	C_p (dimensionless)
0	1.00	100	-0.82
10	0.93	110	-0.80
20	0.65	120	-0.84
30	0.24	130	-0.88
40	-0.54	140	-0.94
50	-0.97	150	-0.90
60	-0.95	160	-0.98
70	-0.82	170	-1.04
80	-0.71	180	-1.08
90	-0.82		

Table 3 (cont'd)

Run Number 15 $N_{Re} = 3.23 \times 10^5$ $N_{ua} = 0.408$ $f = 2.0$ cps

θ	C_p	θ	C_p
(degrees)	(dimensionless)	(degrees)	(dimensionless)
0	1.00	100	-1.76
10	0.95	110	-1.64
20	0.59	120	-1.29
30	0.06	130	-0.95
40	-0.54	140	-0.86
50	-1.42	150	-0.72
60	-1.82	160	-0.73
70	-2.26	170	-0.78
80	-2.26	180	-0.79
90	-2.22		

Table 3 (cont'd)

Run Number 16 $N_{Re} = 3.23 \times 10^5$ $N_{ua} = 0.400$ $f = 3.4$ cps

θ	C_p	θ	C_p
(degrees)	(dimensionless)	(degrees)	(dimensionless)
0	1.00	100	-0.97
10	0.98	110	-0.98
20	0.80	120	-0.93
30	0.35	130	-0.92
40	-0.33	140	-0.95
50	-0.52	150	-0.93
60	-1.28	160	-0.96
70	-1.51	170	-0.92
80	-1.31	180	-0.95
90	-1.12		

Table 3 (cont'd)

Run Number 17 $N_{Re} = 3.23 \times 10^5$ $N_{ua} = 0.387$ $f = 12.2$ cps

θ (degrees)	C_p (dimensionless)	θ (degrees)	C_p (dimensionless)
0	1.00	100	-0.97
10	0.95	110	-0.74
20	0.66	120	-0.76
30	0.14	130	-0.73
40	-0.53	140	-0.77
50	-1.41	150	-0.78
60	-1.94	160	-0.80
70	-1.77	170	-0.78
80	-1.47	180	-0.78
90	-1.43		

Table 3 (cont'd)

Run Number 18 $N_{Re} = 3.23 \times 10^5$ $N_{ua} = 0.390$ $f = 29.0$ cps

θ	C_p	θ	C_p
(degrees)	(dimensionless)	(degrees)	(dimensionless)
0	1.00	80	-1.68
10	0.96	85	-1.46
20	0.69	90	-1.33
30	0.22	95	-1.29
35	0.02	100	-1.22
40	-0.33	110	-1.10
45	-0.87	120	-0.95
50	-1.37	130	-0.96
55	-1.48	140	-0.69
60	-1.59	150	-0.94
65	-1.74	170	-0.97
70	-1.72	180	-0.92
75	-1.72		

Table 3 (cont'd)

Run Number 19 $N_{Re} = 3.43 \times 10^5$ $N_{ua} = 0.378$ $f = 2.0$ cps

θ (degrees)	C_p (dimensionless)	θ (degrees)	C_p (dimensionless)
0	1.00	85	-2.45
10	0.92	90	-2.48
20	0.60	95	-2.47
30	-0.10	100	-2.37
32	-0.09	103	-2.35
34	-0.24	106	-2.29
36	-0.30	110	-2.26
38	-0.43	112	-1.90
40	-0.54	115	-1.62
50	-1.28	118	-1.47
55	-1.60	120	-1.46
60	-1.82	125	-1.20
65	-2.03	130	-0.78
67	-2.16	135	-0.68
70	-2.24	140	-0.78
72	-2.28	150	-0.76
74	-2.32	160	-0.73
77	-2.34	170	-0.73
80	-2.38	180	-0.73

Table 3 (cont'd)

Run Number 20 $N_{Re} = 3.43 \times 10^5$ $N_{ua} = 0.367$ $f = 7.3$ cps

θ (degrees)	C_p (dimensionless)	θ (degrees)	C_p (dimensionless)
0	1.00	82	-1.81
10	0.93	85	-1.72
20	0.59	90	-1.60
30	0.12	92	-1.54
35	-0.20	95	-1.44
37	-0.34	98	-1.27
40	-0.58	100	-1.29
45	-1.16	105	-1.27
48	-1.20	110	-1.26
50	-1.37	115	-1.25
55	-1.74	120	-0.99
60	-1.80	125	-1.26
65	-1.97	130	-1.14
70	-2.20	140	-1.19
72	-2.25	150	-1.26
75	-2.17	160	-1.27
77	-2.15	170	-1.19
80	-2.08	180	-1.21

Table 3 (cont'd)

Run Number 21 $N_{Re} = 3.52 \times 10^5$ $N_{ua} = 0.405$ $f = 2.0$ cps

θ (degrees)	C_p (dimensionless)	θ (degrees)	C_p (dimensionless)
0	1.00	100	-2.40
10	0.87	110	-2.27
20	0.53	120	-1.52
30	0.01	130	-0.76
40	-0.67	140	-0.79
50	-1.43	150	-0.78
60	-1.84	160	-0.79
70	-2.26	170	-0.79
80	-2.26	180	-0.78
90	-2.65		

Table 3 (cont'd)

Run Number 22 $N_{Re} = 3.52 \times 10^5$ $N_{ua} = \text{---}$ $f = 12.4 \text{ cps}$

θ (degrees)	C_p (dimensionless)	θ (degrees)	C_p (dimensionless)
0	1.00	100	-1.44
10	0.89	110	-1.29
20	0.58	120	-1.25
30	0.05	130	-1.26
40	-0.52	140	-1.28
50	-1.29	150	-1.30
60	-1.74	160	-1.30
70	-2.10	170	-1.31
80	-2.13	180	-1.32
90	-1.64		

INITIAL DISTRIBUTION LIST

		No. Copies
1.	Defense Documentation Center Cameron Station Alexandria, Virginia 22314	20
2.	Library U. S. Naval Postgraduate School Monterey, California	2
3.	Commander, Naval Air System Command Department of the Navy Washington, D. C. 20360	1
4.	Commanding Officer and Director David Taylor Model Basin Navy Department (Code 513) Washington, D. C. 20007	2
5.	Chairman, Department of Aeronautics U. S. Naval Postgraduate School Monterey, California	1
6.	Prof James A. Miller Department of Aeronautics U. S. Naval Postgraduate School Monterey, California	20
7.	LT John Cowden Murphy P. O. Box 945 Longview, Texas	1

DOCUMENT CONTROL DATA - R&D

(Security classification of title, body of abstract and indexing annotation must be entered when the overall report is classified)

1. ORIGINATING ACTIVITY (Corporate author) U. S. Naval Postgraduate School Monterey, California		2a. REPORT SECURITY CLASSIFICATION UNCLASSIFIED	
		2b. GROUP	
3. REPORT TITLE THE EFFECTS OF NONSTEADY FLOW ON THE PRESSURE DISTRIBUTION ABOUT A CIRCULAR CYLINDER			
4. DESCRIPTIVE NOTES (Type of report and inclusive dates) Thesis for the Degree of Aeronautical Engineer			
5. AUTHOR(S) (Last name, first name, initial) MURPHY, John C., LT, USN			
6. REPORT DATE May 1966		7a. TOTAL NO. OF PAGES 81	7b. NO. OF REFS 15
8a. CONTRACT OR GRANT NO.		9a. ORIGINATOR'S REPORT NUMBER(S)	
b. PROJECT NO.			
c.		9b. OTHER REPORT NO(S) (Any other numbers that may be assigned this report)	
d.			
10. AVAILABILITY/LIMITATION NOTICES Qualified requesters may obtain copies of this report from DDC for public This document has been approved for public release and sale; its distribution is unlimited. <i>Murphy 1/2/70</i>			
11. SUPPLEMENTARY NOTES		12. SPONSORING MILITARY ACTIVITY Naval Air Systems Command Navy Department Washington, D. C. 20360	
13. ABSTRACT Nonsteady flow is an inherent problem in all fields of aerodynamics. The present work is an experimental investigation of the effects of large scale flow disturbances on the pressure distribution about a transverse circular cylinder. The nonsteady flow in this study was obtained by use of a rotating shutter valve to superimpose a sinusoidally varying velocity component on a mean stream. The frequency of the velocity oscillation covers the range of from 2.0 to 90.0 cycles per second, with amplitudes ranging from 10 to 40 percent of the mean freestream velocity. Both the mean pressure distributions and the instantaneous surface pressure variations were studied for flows in the subcritical and transcritical Reynolds number ranges. Results show that the mean surface pressure is affected most in the high transcritical Reynolds number range at low oscillation frequencies. Here the effect is a reduction of the critical Reynolds number. An effect of low oscillation frequencies on the instantaneous pressure variations consists of a phase shift between the freestream velocity and the velocity near the wall. At high oscillation frequencies this phase shift does not occur, however random fluctuations in the surface pressure are introduced at all angular positions on the cylinder surface.			

14. KEY WORDS	LINK A		LINK B		LINK C	
	ROLE	WT	ROLE	WT	ROLE	WT
Nonsteady Flow Oscillating Flow Circular Cylinder Pressure Distribution						

INSTRUCTIONS

1. **ORIGINATING ACTIVITY:** Enter the name and address of the contractor, subcontractor, grantee, Department of Defense activity or other organization (*corporate author*) issuing the report.
- 2a. **REPORT SECURITY CLASSIFICATION:** Enter the overall security classification of the report. Indicate whether "Restricted Data" is included. Marking is to be in accordance with appropriate security regulations.
- 2b. **GROUP:** Automatic downgrading is specified in DoD Directive 5200.10 and Armed Forces Industrial Manual. Enter the group number. Also, when applicable, show that optional markings have been used for Group 3 and Group 4 as authorized.
3. **REPORT TITLE:** Enter the complete report title in all capital letters. Titles in all cases should be unclassified. If a meaningful title cannot be selected without classification, show title classification in all capitals in parenthesis immediately following the title.
4. **DESCRIPTIVE NOTES:** If appropriate, enter the type of report, e.g., interim, progress, summary, annual, or final. Give the inclusive dates when a specific reporting period is covered.
5. **AUTHOR(S):** Enter the name(s) of author(s) as shown on or in the report. Enter last name, first name, middle initial. If military, show rank and branch of service. The name of the principal author is an absolute minimum requirement.
6. **REPORT DATE:** Enter the date of the report as day, month, year, or month, year. If more than one date appears on the report, use date of publication.
- 7a. **TOTAL NUMBER OF PAGES:** The total page count should follow normal pagination procedures, i.e., enter the number of pages containing information.
- 7b. **NUMBER OF REFERENCES:** Enter the total number of references cited in the report.
- 8a. **CONTRACT OR GRANT NUMBER:** If appropriate, enter the applicable number of the contract or grant under which the report was written.
- 8b, 8c, & 8d. **PROJECT NUMBER:** Enter the appropriate military department identification, such as project number, subproject number, system numbers, task number, etc.
- 9a. **ORIGINATOR'S REPORT NUMBER(S):** Enter the official report number by which the document will be identified and controlled by the originating activity. This number must be unique to this report.
- 9b. **OTHER REPORT NUMBER(S):** If the report has been assigned any other report numbers (*either by the originator or by the sponsor*), also enter this number(s).
10. **AVAILABILITY/LIMITATION NOTICES:** Enter any limitations on further dissemination of the report, other than those

imposed by security classification, using standard statements such as:

- (1) "Qualified requesters may obtain copies of this report from DDC."
- (2) "Foreign announcement and dissemination of this report by DDC is not authorized."
- (3) "U. S. Government agencies may obtain copies of this report directly from DDC. Other qualified DDC users shall request through _____."
- (4) "U. S. military agencies may obtain copies of this report directly from DDC. Other qualified users shall request through _____."
- (5) "All distribution of this report is controlled. Qualified DDC users shall request through _____."

If the report has been furnished to the Office of Technical Services, Department of Commerce, for sale to the public, indicate this fact and enter the price, if known.

11. **SUPPLEMENTARY NOTES:** Use for additional explanatory notes.
12. **SPONSORING MILITARY ACTIVITY:** Enter the name of the departmental project office or laboratory sponsoring (*paying for*) the research and development. Include address.
13. **ABSTRACT:** Enter an abstract giving a brief and factual summary of the document indicative of the report, even though it may also appear elsewhere in the body of the technical report. If additional space is required, a continuation sheet shall be attached.

It is highly desirable that the abstract of classified reports be unclassified. Each paragraph of the abstract shall end with an indication of the military security classification of the information in the paragraph, represented as (TS), (S), (C), or (U).

There is no limitation on the length of the abstract. However, the suggested length is from 150 to 225 words.
14. **KEY WORDS:** Key words are technically meaningful terms or short phrases that characterize a report and may be used as index entries for cataloging the report. Key words must be selected so that no security classification is required. Identifiers, such as equipment model designation, trade name, military project code name, geographic location, may be used as key words but will be followed by an indication of technical context. The assignment of links, roles, and weights is optional.

thesM966

The effects of nonsteady flow on the pre



3 2768 001 92571 2

DUDLEY KNOX LIBRARY